Motion Planning of Legged Robots

Jean-Daniel Boissonnat, Olivier Devillers, Sylvain Lazard

INRIA

INSTITUT NATIONAL DE RECHERCHE EN INFORMATIQUE ET EN AUTOMATIQUE

Motion Planning of Legged Robots

Jean-Daniel Boissonnat , Olivier Devillers , Sylvain Lazard

N˚ 3214

juillet 1997

THÈME 2

ISSN 0249-6399

INRIA
SOPHIA ANTIPOLIS

Motion Planning of Legged Robots

Jean-Daniel Boissonnat , Olivier Devillers , Sylvain Lazard

Thème 2 — Génie logiciel
et calcul symbolique
Projet Prisme

Rapport de recherche n ° 3214 — juillet 1997 — 60 pages

Abstract: We study the problem of computing the free space $\mathcal{F}$ of a simple legged robot called the spider robot. The body of this robot is a single point and the legs are attached to the body. The robot is subject to two constraints: each leg has a maximal extension R (accessibility constraint) and the body of the robot must lie above the convex hull of its feet (stability constraint). Moreover, the robot can only put its feet on some regions, called the foothold regions. The free space $\mathcal{F}$ is the set of positions of the body of the robot such that there exists a set of accessible footholds for which the robot is stable. We present an efficient algorithm that computes $\mathcal{F}$ in $O(n^2 \log n)$ time and $O(n^2\alpha(n))$ space for point footholds where $\alpha(n)$ is an extremely slowly growing function ($\alpha(n) \leq 3$ for any practical value of n). We also present an algorithm to compute $\mathcal{F}$ when the foothold regions are pairwise disjoint polygons with n edges in total. This algorithm computes $\mathcal{F}$ in $O(n^2\alpha_8(n)\log n)$ time using $O(n^2\alpha_8(n))$ space ($\alpha_8(n)$ is also an extremely slowly growing function). These results are close to optimal since $\Omega(n^2)$ is a lower bound for the size of $\mathcal{F}$.

Key-words: Motion planning, legged robots, mobile robot, computational geometry.

(Résumé : tsvp)

Unité de recherche INRIA Sophia Antipolis
2004 route des Lucioles, BP 93, 06902 SOPHIA ANTIPOLIS Cedex (France)
Téléphone : 04 93 65 77 77 – Télécopie : 04 93 65 77 65

Planification de trajectoires de robots à pattes

Résumé : Nous nous intéressons au problème du calcul de l'espace libre $\mathcal{F}$ d'un robot araignée. Un tel robot est un robot à pattes dont le corps est ponctuel et dont les pattes sont attachées au corps. Ce robot est sujet à deux types de contraintes: chaque patte a une élongation maximale R (contrainte d'accessibilité) et le corps du robot doit être situé au dessus de l'enveloppe convexe de ses points d'appui (contrainte de stabilité). De plus, le robot ne peut poser ses pattes que dans certaines régions du plan appelées zones d'appui. L'espace libre $\mathcal{F}$ est l'ensemble des positions du corps du robot telles qu'il existe des points d'appui accessibles pour lesquels le robot est stable. Nous présentons un algorithme pour le calcul de $\mathcal{F}$, lorsque les zones d'appui sont ponctuelles, de complexité en temps $O(n^2 \log n)$ et en espace mémoire $O(n^2\alpha(n))$ où $\alpha(n)$ est une fonction croissant extrêmement lentement ($\alpha(n) \leq 3$ pour toute valeur de n envisageable en pratique). Nous présentons également un algorithme lorsque les zones d'appui sont polygonales. Si n est le nombre total d'arêtes des polygones, cet algorithme calcule $\mathcal{F}$ en temps $O(n^2\alpha_8(n)\log n)$ et en utilisant un espace mémoire $O(n^2\alpha_8(n))$ ($\alpha_8(n)$ est également une fonction croissant extrêmement lentement). Ces résultats sont presque optimaux puisque $\Omega(n^2)$ est une borne inférieure pour la taille de $\mathcal{F}$.

Mots-clé : Planification de trajectoires, robots à pattes, robotique mobile, géométrie algorithmique.

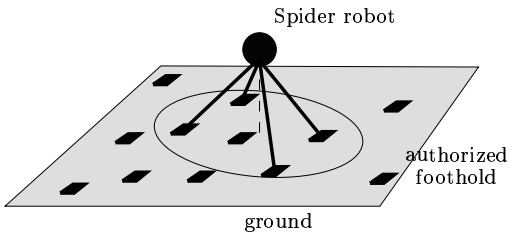

Figure 1: The spider robot.

1 Introduction

Although legged robots have already been studied in robotics [RR84, RR90], only a very few papers consider the motion planning problem amidst obstacles [HNKU84, HK91, BDDP95]. In [HNKU84, HK91] some heuristic approaches are described while, in [BDDP95] efficient and provably correct geometric algorithms are described for a restricted type of legged robots, the so-called spider robots to be defined precisely below, and for finite sets of point footholds.

Compared to the classic piano movers problem, legged robots introduce new types of constraints. We assume that the environment consists of regions in the plane, called *foothold regions*, where the robot can safely put its legs. Then the legged robot must satisfy two different constraints: the accessibility and the stability constraints. A foothold is said *accessible* to a *placement* (position of the body of the robot) if it can be reached by a leg of the robot. A placement is called *stable* if there exist accessible footholds and if the center of mass of the robot lies above the convex hull of these accessible footholds. The set of stable placements is clearly the relevant information for planning the motion of a legged robot: we call this set *the free space* of the legged robot. A legged robot has at least four legs, three legs ensure the stability of a placement and a fourth leg permits the motion of the robot.

A first simple instance of a legged robot is the *spider robot*. The spider robot has been inspired by the Ambler, developed at Carnegie Mellon University [JW89]. The body of the spider robot is a single point: all its legs are attached to the body and can reach any foothold at distance less than a constant R from the body (see Figure 1). The problem of planning the motion of a spider robot in an environment of point footholds has already been studied by Boissonnat et al. [BDDP95]. However their method assumes that the set of footholds is a finite set of points and cannot be generalized to more complex environments. This paper proposes a new method to compute the free space of a spider robot based on a transformation between this

problem and the problem of moving a half-disk amidst obstacles. The algorithm is simpler than the one described in [BDDP95] and the method can be extended to the case of polygonal foothold regions. Once the free space has been computed, it can be used to find trajectories and sequences of legs assignments as described in [BDDP95].

The paper is organized as follows: some notations and results of [BDDP95] are recalled in the next section. Section 3 shows the transformation between the spider robot problem and the half-disk problem. We present in Section 4 an algorithm that computes the free space of a spider robot for point footholds. Section 5 shows how the algorithm can be extended to polygonal foothold regions.

2 Notations and previous results

We introduce some notations. In Sections 2, 3 and 4, $\mathcal{S}$ is a discrete set of distinct point footholds $\{s_1, \ldots, s_n\}$ in the Euclidean plane. G denotes the body of the robot and R is the maximal length of each leg attached to G. For convenience and without loss of generality, we assume that G belongs to the plane containing the footholds (G can be seen as the orthogonal projection of the body of the robot onto the plane containing the footholds). The free space $\mathcal{F}$ is the set of all stable placements. A placement is said at the limit of stability if it lies on the boundary of the convex hull of the accessible point footholds. Notice that $\mathcal{F}$ is a closed set and contains the placements at the limit of stability. Let $\delta(\mathcal{F})$ denote the boundary of $\mathcal{F}$ and C_i denote the circle of radius R centered at s_i. $\mathcal{A}$ is the arrangement of the circles C_i for $1 \leq i \leq n$, i.e. the subdivision of the plane induced by the circles. This arrangement plays an important role in our problem and we will express the complexity results in term of $|\mathcal{A}|$, the size of $\mathcal{A}$. In the worst-case, $|\mathcal{A}| = \Theta(n^2)$ but if k denotes the maximum number of disks $D(s_i, R)$ that can cover a point of the plane, it can be shown that $|\mathcal{A}| = O(kn)$ [Sha91]. Clearly k is not larger than n and in case of sparse footholds $|\mathcal{A}|$ may be linearly related to the number of footholds. Let $S^1 = \mathbb{R}/2\pi\mathbb{Z}$. Let $\mathrm{CH}(\mathcal{E})$ denote the convex hull of a set $\mathcal{E}$, $compl(\mathcal{E})$ the complementary set of $\mathcal{E}$ and $int(\mathcal{E})$ the interior of $\mathcal{E}$. We say in the sequel that two objects *properly intersect* if and only if their relative interiors intersect.

The algorithm described in [BDDP95] is based on the following observation: in a cell Γ of $\mathcal{A}$, the set of footholds that can be reached by the robot is fixed; the portion of Γ that belongs to $\mathcal{F}$ is exactly the intersection of Γ with the convex hull of the footholds that can be reached from Γ. Therefore, the edges of $\delta(\mathcal{F})$ are either circular arcs belonging to $\mathcal{A}$ or portions of line segments joining two footholds; moreover a

vertex of $\delta(\mathcal{F})$ incident to two straight line edges is a foothold (see Figure 2). The complexity of $\mathcal{F}$ has been proved to be $|\mathcal{F}| = \Theta(|\mathcal{A}|)$ [BDDP95].

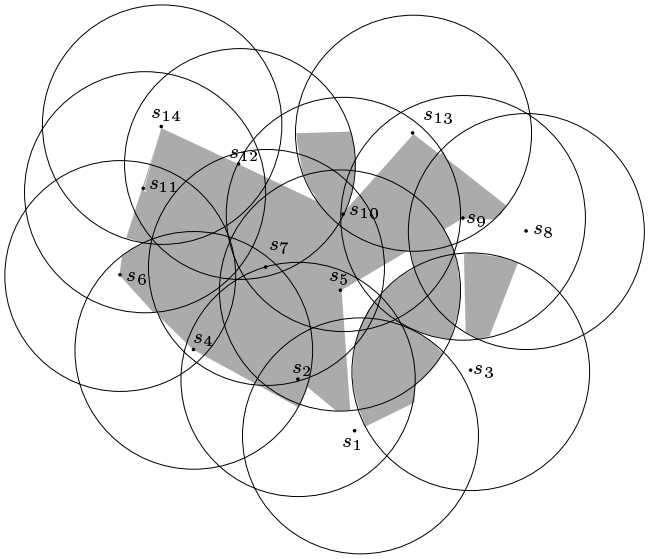

Figure 2: An example of the free space of a spider robot.

The algorithm presented in [BDDP95] computes the free space $\mathcal{F}$ in $O(|\mathcal{A}| \log n)$ time. It uses sophisticated data structures allowing the off-line maintenance of convex hulls.

The algorithm described in this paper has the same time complexity, uses simple data structures and can be extended to the case where the set $\mathcal{S}$ of footholds is a set of polygonal regions and not simply a set of points. For simplicity, we consider first the case of point footholds and postpone the discussion on polygonal footholds to Section 5.

General position assumption

To simplify the presentation of this paper, we make some general position assumptions.

No two footholds lie at distance exactly $2R$. This hypothesis is not really restrictive. Indeed, if the robot uses two such footholds, it is at the midle of the two footholds and cannot move.

No three footholds have a circumscribing circle of radius R. Such a configuration will be relevant only for a placement of the robot at the center of the circle and the robot cannot move using such a position for its legs.

We also assume that the line joining two footholds is not exactly at distance R from another foothold. This hypothesis forbids the boundary of $\mathcal{F}$ to contain edges that degenerate into points.

All these hypotheses concern some special points of $\mathcal{F}$, isolated points or singular points on its boundary, and can be removed by a careful analysis.

3 From spider robots to half-disk robots

In this section, we establish the connection between the free space of the spider robot and the free space of a half-disk robot moving by translation and rotation amidst n point obstacles.

Theorem 1 *The spider robot does not admit a stable placement at point P if and only if there exists a half-disk (of radius R) centered at P that does not contain any foothold of $\mathcal{S}$ (see Figure 3).*

Proof: A placement of the spider robot is not stable if and only if the convex hull of all the reachable footholds does not contain the body G of the robot. That is equivalent to: there exists a closed half-disk of radius R centered at G which does not contain any foothold (see Figure 3). □

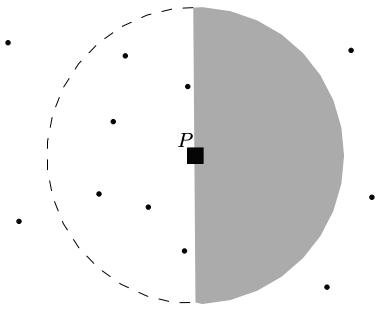

Figure 3: A placement which is not stable.

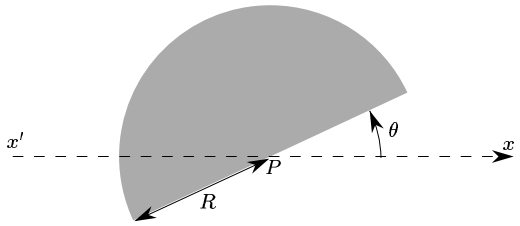

Figure 4: $HD(P,\theta)$.

Definition 2 *Let $HD(P,\theta)$ be the half-disk of radius R centered at P (see Figure 4) defined by:*

$$\begin{cases} (x-x_P)^2+(y-y_P)^2 \leq R^2 \\ (x-x_P)\sin\theta-(y-y_P)\cos\theta \leq 0 \end{cases}$$

Definition 3 *$\forall s_i \in \mathcal{S}$ $(1 \leq i \leq n)$ let us define:*

$$\mathcal{H}_i = \{(P,\theta) \in I\!R^2 \times S^1 \ / \ P \in HD(s_i,\theta)\}$$

$$\mathcal{H} = \bigcup_{i=1}^{n} \mathcal{H}_i$$

$$\mathcal{C}_i = C_i \times S^1$$

$\mathcal{H}_i$ will be called the helicoidal volume centered at s_i (see Figure 5).

Notice the typographical distinction between the circle C_i defined in $I\!R^2$ and the torus $\mathcal{C}_i$ defined in $I\!R^2 \times S^1$. For convenience, we will often identify S^1 and the interval $[0,2\pi]$ of $I\!R$. This allows to draw objects of $I\!R^2 \times S^1$ in $I\!R^3$ and to speak of the θ-axis. Π_{θ_0} denote the "plane" $\{(P,\theta) \in I\!R^2 \times S^1 \ / \ \theta = \theta_0\}$.

Definition 4 *We define the free space $\mathcal{L}$ of a half-disk robot moving by translation and rotation amidst the set of obstacles $\mathcal{S}$ as the set of $(P,\theta) \in I\!R^2 \times S^1$ such that the half-disk $HD(P,\theta+\pi)$ and $\mathcal{S}$ have an empty intersection.*

Proposition 5 $\mathcal{L} = compl(\mathcal{H})$.

Proof: $\forall \theta \in S^1$, the set $\mathcal{L} \cap \Pi_\theta$ is the free space of the half disk $HD(P,\theta+\pi)$ moving by translation only, amidst the obstacle $s_1,\ldots,s_n$. Thus, $\mathcal{L} \cap \Pi_\theta$ is the complementary

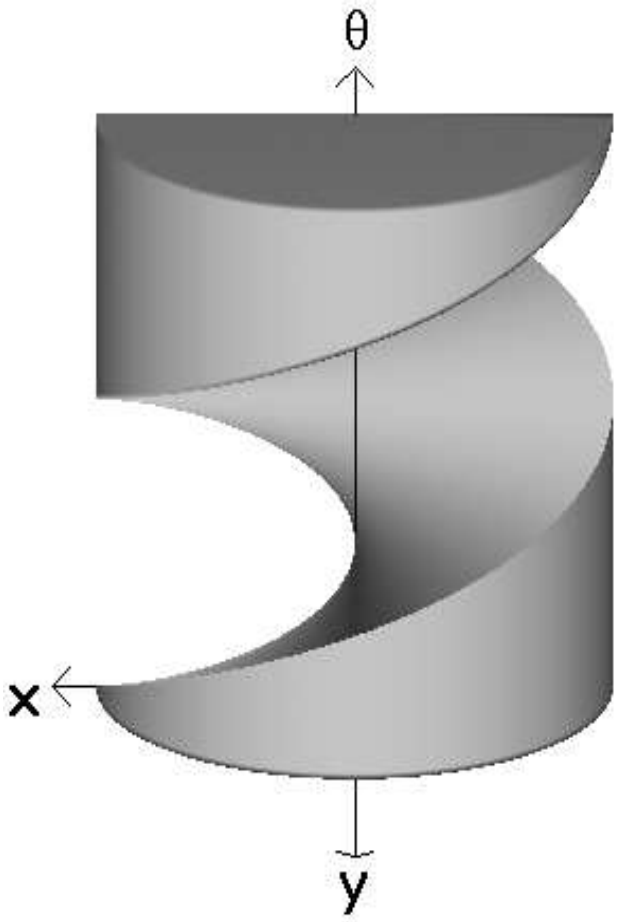

Figure 5: Helicoidal volume $\mathcal{H}_i$.

set of the union of the n Minkowski's sums $s_i \ominus HD(O, \theta + \pi) = HD(s_i, \theta)$ where O is the origin of the reference frame. Therefore, we have:

$$\forall \theta \in S^1 \quad \mathcal{L} \cap \Pi_\theta = compl(\bigcup_{1 \leq i \leq n} HD(s_i, \theta))$$

and Definition 3 yields the result. □

Let $p_{//\theta}$ denote the mapping (called "orthogonal projection"): $\mathbb{R}^2 \times S^1 \longrightarrow \mathbb{R}^2, (P, \theta) \mapsto P$.

Theorem 6 $\mathcal{F} = compl(p_{//\theta}(compl(\mathcal{H})))$

Proof: According to Theorem 1 and Definitions 2 and 4, $\mathcal{F} = compl(p_{//\theta}(\mathcal{L}))$. The result then follows from Proposition 5. □

Remark 7 $compl(p_{//\theta}(compl(\mathcal{H}))) \times S^1$ is the largest "cylinder" included in $\mathcal{H}$, whose axis is parallel to the θ-axis (see Figure 6). The basis of this cylinder is $\mathcal{F}$.

Remark 8 Among the previously defined objects, notice which one are closed or open sets. $HD(s_i, \theta)$ and $\mathcal{H}_i$ are closed by definition, $\mathcal{H}$ is closed (union of closed sets), $\mathcal{L}$ is open (complementary of $\mathcal{H}$), $compl(\mathcal{F})$ is open (projection of $\mathcal{L}$) and $\mathcal{F}$ is closed (complementary of $compl(\mathcal{F})$).

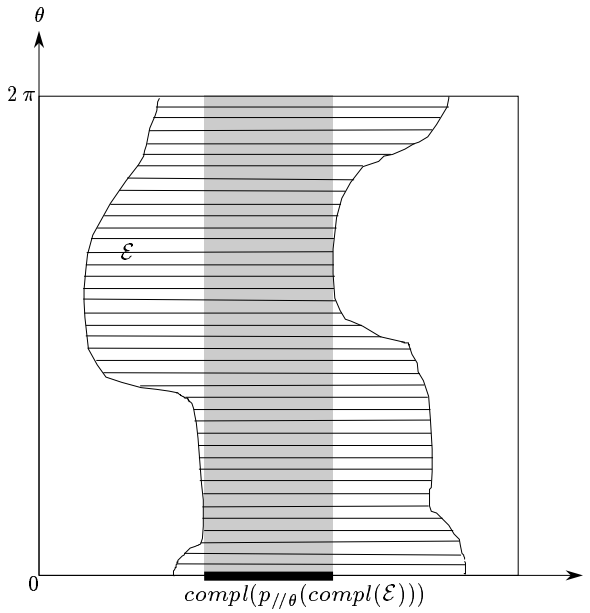

Figure 6: $compl(p_{//\theta}(compl(\mathcal{E})))$.

Remark 9 The results of this section do not depend on the fact that the footholds are points. For more general foothold regions, we simply need to replace the helicoidal volumes by their analogs. This will be done in Section 5.

4 Computation of $\mathcal{F}$

In this section, we propose an algorithm to compute $\mathcal{F}$ based on Theorem 6.

A first attempt to use Theorem 6 may consist in computing $\mathcal{L}$ and to project its complementary on to the horizontal plane. The motion planning of a convex polygonal robot in a polygonal environment has been extensively studied (see for example [KS90, KST97]). Such algorithms can be generalized to plan the motion of a half-disk. It should lead to an algorithm of complexity $O(n\lambda_s(n)\log n)$, where $\lambda_s(n)$ is an almost linear function of n. The projection can be done using classical techniques, such as projecting all the faces of $\mathcal{L}$ and computing their union. Since the complexity of the 3D object $\mathcal{L}$ is not directly related to the complexity of its projection, this approach do not provide a combinatorial bound on $\mathcal{F}$. However, assuming $|\mathcal{F}| = O(\lambda_s(|\mathcal{A}|))$ (which will be proved in this paper) the time complexity the algortihm of Kedem et al. is $O(n\lambda_s(n)\log n + \lambda_s(|\mathcal{A}|)\log^2 n)$.

In this paper, we present a direct computation of $\mathcal{F}$. This approach provides an upper bound on the size of $\mathcal{F}$, namely $|\mathcal{F}| = O(\lambda_s(|\mathcal{A}|))$. It also provides an algorithm to compute $\mathcal{F}$ in $O(\lambda_s(|\mathcal{A}|)\log n)$ time. As in [SS87] and contrary to [KST97], the algorithm proposed here is sensitive to $|\mathcal{A}|$ which is usually less than quadratic. Another advantage of our direct computation, is to avoid the explicit construction of the 3D object $\mathcal{L}$ which is useless for our application. Our algorithm manipulates only two dimensional arrangements or lower envelopes and we provide a detailed description of the curves involved in the construction.

Let us now detail the computation of $\mathcal{F}$ in the case of point footholds. We know that each arc of the boundary $\delta(\mathcal{F})$ of $\mathcal{F}$ is either a straight line segment belonging to a line joining two footholds or an arc of a circle C_i (see Section 2). The circular arcs $\delta(\mathcal{F}) \cap C_i$ are computed first (Sections 4.1, 4.2 and 4.3) and linked together with the line segments in a second step (Sections 4.4 and 4.5).

4.1 Computation of $\delta(\mathcal{F}) \cap \mathcal{A}$

We compute the contribution of each circle C_{i_0}, $i_0 = 1, \ldots, n$, to $\delta(\mathcal{F})$ in turn. $\mathcal{C}_{i_0}$ is the torus $C_{i_0} \times S^1$. We assume that C_{i_0} is parameterized by u and $\mathcal{C}_{i_0}$ by (u, θ).

Since $\mathcal{F}$ is a closed set, the contribution of C_{i_0} to $\delta(\mathcal{F})$ is the difference between the contribution of C_{i_0} to $\mathcal{F}$ and the contribution of C_{i_0} to the interior of $\mathcal{F}$. According to Theorem 6, $\mathcal{F} \cap C_{i_0} = compl(p_{//\theta}(compl(\mathcal{H} \cap \mathcal{C}_{i_0})))$ and in general position $int(\mathcal{F}) \cap C_{i_0} = compl(p_{//\theta}(compl(int(\mathcal{H}) \cap \mathcal{C}_{i_0})))$. Let $\mathcal{Z}_i$ denote $\mathcal{H}_i \cap \mathcal{C}_{i_0}$ (see Figure 7). Clearly, $\mathcal{H} \cap \mathcal{C}_{i_0} = \cup_i \mathcal{Z}_i$. On the other hand, $int(\mathcal{H}) \cap \mathcal{C}_{i_0} = int(\cup_{i \neq i_0} \mathcal{Z}_i)$. Indeed, $int(\mathcal{H}_{i_0}) \cap \mathcal{C}_{i_0} = \emptyset$ and, according to the general position assumption,

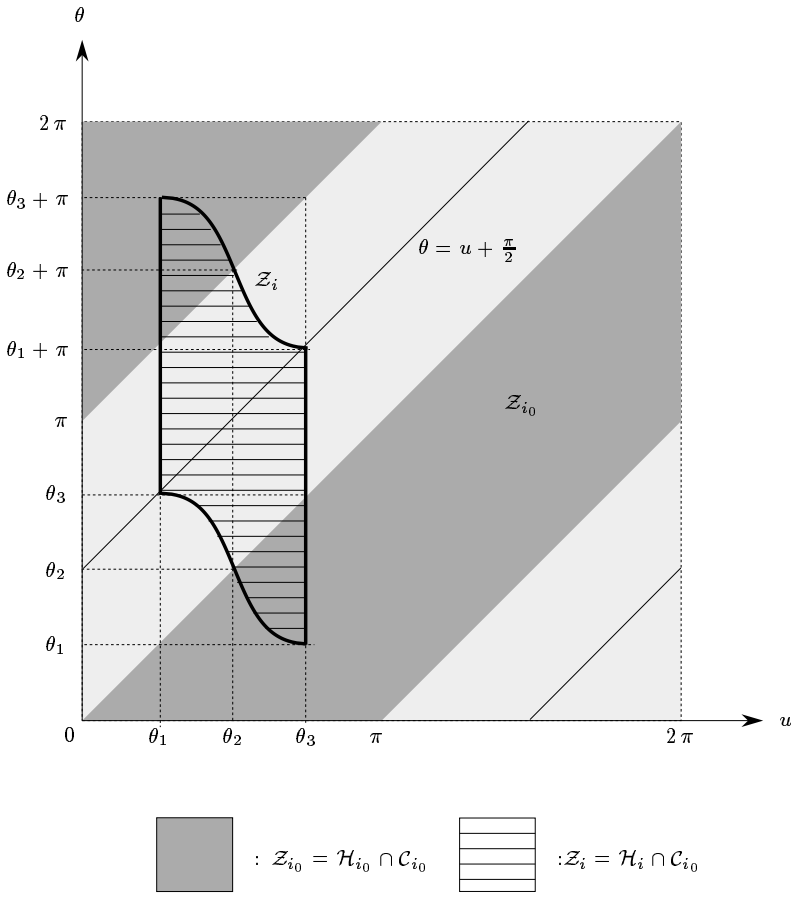

Figure 7: Intersection of $\mathcal{H}_i$ with $\mathcal{C}_{i_0}$ for $\|s_{i_0}s_i\| = \sqrt{2}\,R$ and $\angle(\vec{x}, \overrightarrow{s_{i_0}s_i}) = \theta_2 = \pi/2$.

for $i \neq i_0$, $int(\mathcal{H}_i) \cap \mathcal{C}_{i_0} = int(\mathcal{Z}_i)$ (notice that $int(\mathcal{H}_i)$ is the interior of $\mathcal{H}_i$ in $\mathbb{R}^2 \times S^1$ but $int(\mathcal{Z}_i)$ denotes the interior of $\mathcal{Z}_i$ in $S^1 \times S^1$). It follows that $\mathcal{F} \cap C_{i_0}$ $= compl(p_{//\theta}(compl(\cup_i \mathcal{Z}_i)))$ and $int(\mathcal{F}) \cap C_{i_0} = int(compl(p_{//\theta}(compl(\cup_{i\neq i_0} \mathcal{Z}_i))))$. Therefore,

$$\delta(\mathcal{F}) \cap C_{i_0} = compl(p_{//\theta}(compl(\cup_i \mathcal{Z}_i))) \setminus int(compl(p_{//\theta}(compl(\cup_{i\neq i_0} \mathcal{Z}_i)))).$$

Thus, the contribution of C_{i_0} to $\delta(\mathcal{F})$ comes from the computation of $\cup_i \mathcal{Z}_i$ and $\cup_{i\neq i_0} \mathcal{Z}_i$.

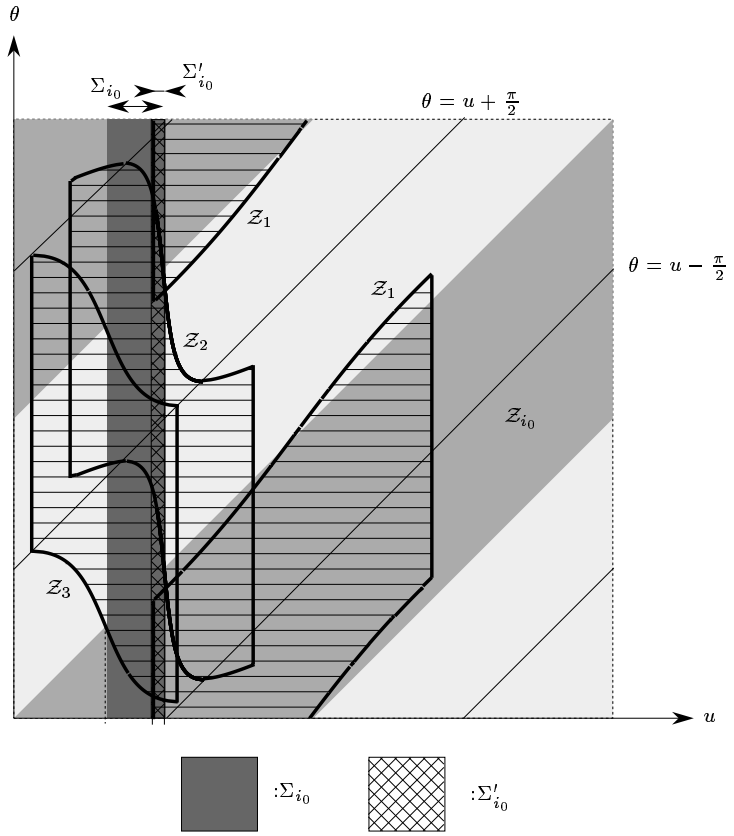

Figure 8: Contribution of C_{i_0} to $\delta(\mathcal{F})$ ($0 < \|s_1 s_{i_0}\| < R$, $R \leq \|s_2 s_{i_0}\| < \sqrt{2}\,R$, $\sqrt{2}\,R \leq \|s_3 s_{i_0}\| < 2R$).

Geometrically, $compl(p_{//\theta}(compl(\cup_i \mathcal{Z}_i)))$ is the orthogonal projection of the largest vertical strip Σ_{i_0} included in $\cup_i \mathcal{Z}_i$. Similarly, $compl(p_{//\theta}(compl(\cup_{i\neq i_0} \mathcal{Z}_i)))$ is the projection, along a direction parallel to the θ-axis, of the largest vertical strip Σ'_{i_0} included in $\cup_{i\neq i_0} \mathcal{Z}_i$. Thus, $\delta(\mathcal{F}) \cap C_{i_0}$ is the vertical projection onto C_{i_0} of the vertical strip $\Sigma_{i_0} \setminus int(\Sigma'_{i_0})$ (see Figure 8).

In order to compute $\mathcal{F}$ efficiently, we need to compute the union of the regions $\mathcal{Z}_i$ efficiently. More precisely, we will show that the union of the regions $\mathcal{Z}_i$ can be computed in $O(k_{i_0} \log k_{i_0})$ time where k_{i_0} is the number of helicoidal volumes $\mathcal{H}_i$ intersecting $\mathcal{C}_{i_0}$.

This is possible because the $\mathcal{Z}_i$ have a special shape that allows to reduce the computation of their union to the computation of a small number of lower envelopes of curves drawn on $\mathcal{C}_{i_0}$ with the property that two of them intersect at most once. The geometric properties of the $\mathcal{Z}_i$ are discussed in Section 4.2 and, in Section 4.3, we present and analyze the algorithm for constructing $\delta(\mathcal{F}) \cap C_{i_0}$.

4.2 Properties of the $\mathcal{Z}_i$

We study here the regions $\mathcal{Z}_i = \mathcal{H}_i \cap \mathcal{C}_{i_0}$. For convenience, we will use the vocabulary of the plane when describing objects on the torus $\mathcal{C}_{i_0}$. For instance, the curve drawn on the torus $\mathcal{C}_{i_0}$ with equation

$$a\,\theta + b\,u + c = 0$$

will be called a line. The line $u = u_0$ will be called vertical and oriented according to increasing θ. Lower and upper will refer to this orientation. The discussion below considers only non empty regions $\mathcal{Z}_i$.

We introduce here a few notations. Let $HC_i(\theta)$ be the half-circle of the boundary of $HD(s_i, \theta)$, i.e. $HC_i(\theta) = C_i \cap HD(s_i, \theta)$. Let $r_i(\theta)$ be the radius of C_i that makes an angle θ with the x-axis, i.e. $r_i(\theta) = \{s_i + \lambda \vec{u}_\theta \,/\, \lambda \in [0, R]\}$ where $\vec{u}_\theta$ is the unit vector whose polar angle is θ. The boundary of $\mathcal{H}_i$ is composed of the three following patches:

$$\begin{aligned} \mathcal{T}_i &= \{(HC_i(\theta), \theta) \in I\!R^2 \times S^1\} \\ \mathcal{R}_i^+ &= \{(r_i(\theta), \theta) \in I\!R^2 \times S^1\} \\ \mathcal{R}_i^- &= \{(r_i(\theta + \pi), \theta) \in I\!R^2 \times S^1\} \end{aligned}$$

Proposition 10 *The region $\mathcal{Z}_{i_0}$ is the subset of $\mathcal{C}_{i_0}$ defined by $\{(u, \theta) \in S^1 \times S^1 \,/\, \theta \leq u \leq \theta + \pi\}$ and shown in dark grey in Figure 7.*

Proof: For any $\theta_0 \in S^1$ the intersection between $\mathcal{H}_{i_0}$ and the "plane" $\{(P, \theta) \in I\!R^2 \times S^1 \,/\, \theta = \theta_0\}$ is the half-disk $HD(s_{i_0}, \theta_0)$. □

Proposition 11 *For $i \neq i_0$, $\mathcal{Z}_i$ is a connected region bounded by two vertical line segments of length π, and two curved edges ρ_i^+ and ρ_i^- that are translated copies of one another. Specifically $\rho_i^+ = \rho_i^- + (0, 0, \pi)$.*

Proof: Consider the two points of intersection between the circles C_{i_0} and C_i ($i \neq i_0$). Let $u = \theta_1$ and $u = \theta_3$ be the parameters of these two points using the natural

parameterization of C_{i_0} (see Figure 9). The half circle $HC_i(\theta)$ intersects C_{i_0} at $u = \theta_3$ (resp. at $u = \theta_1$) for $\theta \in [\theta_1, \theta_1 + \pi]$ (resp. for $\theta \in [\theta_3, \theta_3 + \pi]$) (see Figure 9). Hence, $\mathcal{T}_i \cap \mathcal{C}_{i_0}$ consists of the two vertical line segments of length π $\{(u, \theta) \in \{\theta_3\} \times [\theta_1, \theta_1 + \pi]\}$ and $\{(u, \theta) \in \{\theta_1\} \times [\theta_3, \theta_3 + \pi]\}$ (see Figure 7).

On the other hand, the definitions of $\mathcal{R}_i^+$ and $\mathcal{R}_i^-$ clearly yield that $\mathcal{R}_i^+ = \mathcal{R}_i^- + (0, 0, \pi)$. Therefore, the two curved edges $\rho_i^- = \mathcal{R}_i^- \cap \mathcal{C}_{i_0}$ and $\rho_i^+ = \mathcal{R}_i^+ \cap \mathcal{C}_{i_0}$ are translated copies of one another (see Figure 7). □

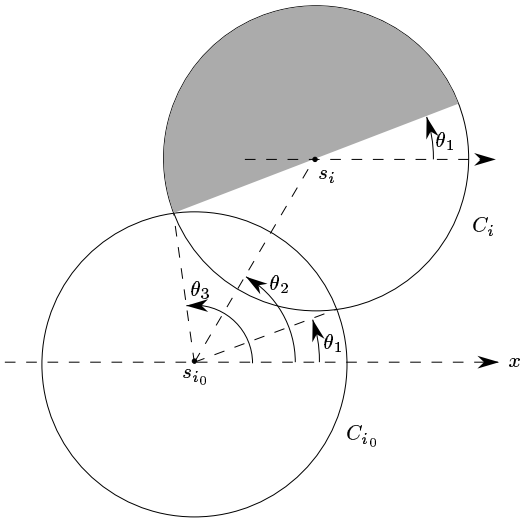

Figure 9: Definition of θ_1, θ_2 and θ_3 ($0 < \|s_{i_0} s_i\| < 2R$).

When not necessary, we will not specify which one of ρ_i^+ or ρ_i^- (resp. $\mathcal{R}_i^+$ or $\mathcal{R}_i^-$) is considered, and we will simply use the notation ρ_i (resp. $\mathcal{R}_i$). In addition to the previous notations, ρ_i' or ρ_i^j will denote a portion of ρ_i.

Proposition 12 *Let ρ_i' and ρ_j' be some connected portions of ρ_i and ρ_j respectively. If ρ_i' or ρ_j' is the graph of a function of θ and if this function is defined over a θ-interval smaller than π, then ρ_i' and ρ_j' intersect at most once.*

Proof: Let (u_I, θ_I) be a point of intersection between ρ_i' and ρ_j' and I be the point of the circle C_{i_0} with parameter u_I. Since ρ_i' is a portion of the intersection between $\mathcal{C}_{i_0}$ and $\mathcal{R}_i$, I is a point of intersection between C_{i_0} and the diameter of $HD(s_i, \theta_I)$. Therefore, the line passing through s_i and I has slope θ_I.

By applying the same argument to ρ'_j, we obtain that s_i and s_j belong to the same straight line of slope θ_I. Therefore, if ρ'_i and ρ'_j intersect twice, at (u_I, θ_I) and (u_J, θ_J), then $\theta_I = \theta_J[\pi]$. If ρ'_i or ρ'_j is defined over a θ-interval smaller than π, then $\theta_I = \theta_J[2\pi]$. Furthermore, if ρ'_i or ρ'_j is the graph of a function of θ, then (u_I, θ_I) and (u_J, θ_I) are equal. □

Proposition 13 *If $\sqrt{2}\,R \leq \|s_{i_0}s_i\| < 2R$, ρ_i is the graph of a function of θ defined over a θ-interval smaller than π.*

Proof: If $\sqrt{2}\,R \leq \|s_{i_0}s_i\| < 2R$, $r_i(\theta)$ (and also $r_i(\theta+\pi)$) intersects C_{i_0} in at most one point, which proves that ρ_i is the graph of a function of θ. Furthermore, the θ-interval where ρ_i is defined is clearly smaller than π. □

As a consequence of Propositions 12 and 13, if the distances $\|s_{i_0}s_i\|$ and $\|s_{i_0}s_j\|$ belong to $[\sqrt{2}\,R, 2R)$, ρ_i and ρ_j intersect at most once.

Proposition 14 *If $\sqrt{2}\,R \leq \|s_{i_0}s_i\| < 2R$, the line $\theta = u + \frac{\pi}{2}$ properly intersects $\mathcal{Z}_i$. Furthermore, the lines $\theta = u \pm \frac{\pi}{2}$ properly intersect neither ρ_i^+ nor ρ_i^-.*

Proof: Let (u_P, θ_P) be a point of ρ_i and P the point of C_{i_0} with parameter u_P. By definition, $u_P = \angle(\vec{x}, \overrightarrow{s_{i_0}P})$ $[2\pi]$ and $\theta_P = \angle(\vec{x}, \overrightarrow{s_iP})$ $[\pi]$ (see Figure 10). Let $\gamma = \angle(\overrightarrow{Ps_{i_0}}, \overrightarrow{Ps_i})$ $[2\pi]$. When $\sqrt{2}\,R \leq \|s_{i_0}s_i\| < 2R$, then $\gamma \in [\frac{\pi}{2}, \frac{3\pi}{2}]$ and $\gamma = \frac{\pi}{2}$ $[\pi]$ only when $\|s_{i_0}s_i\| = \sqrt{2}\,R$ and (u_P, θ_P) is an endpoint of ρ_i. Thus, if (u_P, θ_P) is not an endpoint of ρ_i, $\theta_P - u_P \neq \frac{\pi}{2}[\pi]$ because $\theta_P - u_P = \gamma[\pi]$. Therefore, the lines $\theta = u \pm \frac{\pi}{2}$ intersect neither ρ_i^+ nor ρ_i^-, except possibly at their endpoints.

It remains to show that the line $\theta = u + \frac{\pi}{2}$ properly intersects $\mathcal{Z}_i$. This follows from the fact that the point of $\mathcal{C}_{i_0}$ $(\theta_2, \theta_2 + \frac{\pi}{2})$, where $\theta_2 = \angle(\vec{x}, \overrightarrow{s_{i_0}s_i})$ $[2\pi]$, belongs to the line $\theta = u + \frac{\pi}{2}$ and also to the relative interior of $\mathcal{Z}_i$ if $R \leq \|s_{i_0}s_i\| < 2R$ (see Figures 7 and 11). □

Proposition 15 *If $0 < \|s_{i_0}s_i\| < R$ (resp. $R \leq \|s_{i_0}s_i\| < \sqrt{2}\,R$), ρ_i can be subdivided into two (resp. three) sub-curves denoted ρ_i^k, $k \in \{1,2\}$ (resp. $k \in \{1,2,3\}$), such that each piece is the graph of a function of θ defined over a θ-interval smaller than π.*

Proof:

Case 1 : $0 < \|s_{i_0}s_i\| < R$.

Any radius of C_i intersects C_{i_0} at most once. Hence, ρ_i is the graph of a function of θ.

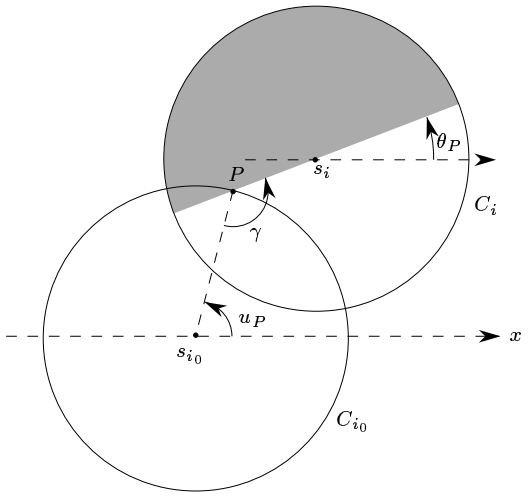

Figure 10: For the definition of P, u_P, θ_P, γ.

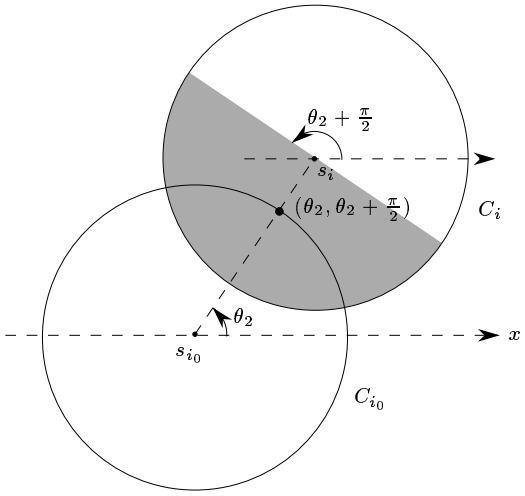

Figure 11: Section of $\mathcal{H}_i$ and $\mathcal{C}_{i_0}$ by the "plane" $\Pi_{\theta_2+\frac{\pi}{2}}$.

ρ_i is defined over a θ-interval greater than π but smaller than 2π. By splitting this interval in two equal parts, we split ρ_i in two sub-curves ρ_i^1 and ρ_i^2 which are defined over a θ-interval smaller than π (see $\mathcal{Z}_1$ in Figure 8).

Case 2 : $R \leq \|s_{i_0} s_i\| < \sqrt{2}\, R$.

In that case, the θ-interval where $r_i(\theta)$ (or $r_i(\theta+\pi)$) intersects C_{i_0} is smaller than π, which implies that ρ_i is defined over a θ-interval smaller than π.

It may exist two points of intersection between $r_i(\theta)$ and C_{i_0}. In order to overcome this difficulty, we split $r_i(\theta)$ into two segments (of fixed lengths, independently of θ) as follows (see Figure 12). Let $r_i(\theta_T)$ be one of the two radii of C_i that are tangent to C_{i_0}. Let T be the point where $r_i(\theta_T)$ and C_{i_0} are tangent and $T(\theta)$ the point of $r_i(\theta)$ which is identical to T when $\theta = \theta_T$. Cutting $r_i(\theta)$ at $T(\theta)$ defines two sub-radii $r_i'(\theta)$ and $r_i''(\theta)$ that intersect C_{i_0} in at most one point each; without loss of generality, let $r_i''(\theta)$ denote the sub-radius not connected to s_i. We define

$$\mathcal{R}_i^{'+} = \{(r_i'(\theta), \theta)\} \qquad \mathcal{R}_i^{'-} = \{(r_i'(\theta+\pi), \theta)\}$$

$$\mathcal{R}_i^{''+} = \{(r_i''(\theta), \theta)\} \qquad \mathcal{R}_i^{''-} = \{(r_i''(\theta+\pi), \theta)\}$$

The intersection of $\mathcal{R}_i^{'}$ (i.e. $\mathcal{R}_i^{'+}$ or $\mathcal{R}_i^{'-}$) and $\mathcal{C}_{i_0}$ consists of one continuous curve ρ_i^2, which is the graph of a decreasing function of θ. The intersection of $\mathcal{R}_i^{''}$ and $\mathcal{C}_{i_0}$ consists of two continuous curves ρ_i^1 and ρ_i^3, which are both graphs of increasing functions of θ (see $\mathcal{Z}_2$ on Figure 8). □

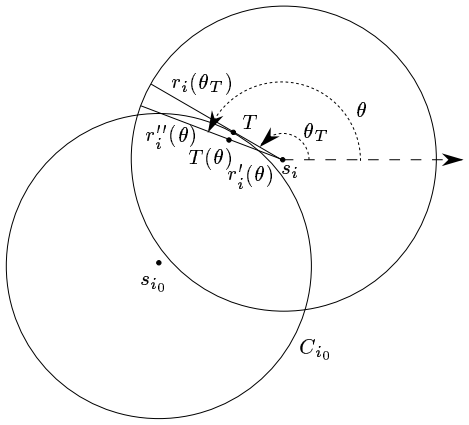

Figure 12: For the definition of T, $T(\theta)$, $r_i'(\theta)$, $r_i''(\theta)$.

As $\mathcal{R}_i^{'+} = \mathcal{R}_i^{'-} + (0,0,\pi)$ and $\mathcal{R}_i^{''+} = \mathcal{R}_i^{''-} + (0,0,\pi)$, ρ_i^{k+} and ρ_i^{k-} are translated copies of one another by vector $(0,0,\pi)$. We denote $\mathcal{Z}_i^k$ the sub-region of $\mathcal{Z}_i$ below ρ_i^{k+} and above ρ_i^{k-}.

Proposition 16 *If $0 < \|s_{i_0}s_i\| < R$, the line $\theta = u - \frac{\pi}{2}$ properly intersects $\mathcal{Z}_i^1$ and $\mathcal{Z}_i^2$. Furthermore, the lines $\theta = u \pm \frac{\pi}{2}$ properly intersect none of the edges ρ_i^{1+}, ρ_i^{1-}, ρ_i^{2+} and ρ_i^{2-}.*

If $R \leq \|s_{i_0}s_i\| < \sqrt{2}\,R$, the line $\theta = u + \frac{\pi}{2}$ (resp. $\theta = u - \frac{\pi}{2}$) properly intersects $\mathcal{Z}_i^2$ (resp. $\mathcal{Z}_i^1$ and $\mathcal{Z}_i^3$). Furthermore, the lines $\theta = u \pm \frac{\pi}{2}$ properly intersect none of the edges ρ_i^{1+}, ρ_i^{1-}, ρ_i^{2+}, ρ_i^{2-}, ρ_i^{3+} and ρ_i^{3-}.

Proof: The proof is similar to the proof of Proposition 14. Let (u_P, θ_P) denote a point of a curve ρ_i^k. P is the point of C_{i_0} with parameter u_P and $\gamma = \angle(\overrightarrow{Ps_{i_0}}, \overrightarrow{Ps_i})$ $[2\pi]$. We show that $\gamma \neq \frac{\pi}{2}$ $[\pi]$, except possibly when (u_P, θ_P) is an endpoint of ρ_i^k. As $\gamma = \theta_P - u_P[\pi]$, it follows that the lines $\theta = u \pm \frac{\pi}{2}$ intersect neither ρ_i^{k+} nor ρ_i^{k-}, except possibly at their endpoints.

Case 1 : $0 < \|s_{i_0}s_i\| < R$.

$\gamma \in (-\frac{\pi}{2}, \frac{\pi}{2})$ for any $P \in C_{i_0}$. Thus, the lines $\theta = u \pm \frac{\pi}{2}$ properly intersect neither ρ_i^+ nor ρ_i^-. Therefore, the same result holds for the sub-curves $\rho_i^{k\pm}$ of $\rho_i^\pm$. Moreover (see Figure 11), the point $(\theta_2, \theta_2 - \frac{\pi}{2}) \in \mathcal{C}_{i_0}$ belongs to the relative interior of $\mathcal{Z}_i$. Therefore, the line $\theta = u - \frac{\pi}{2}$ properly intersects $\mathcal{Z}_i$. It follows that the line $\theta = u - \frac{\pi}{2}$ properly intersects $\mathcal{Z}_i^1$ and $\mathcal{Z}_i^2$ because it properly intersects neither ρ_i^+ nor ρ_i^-.

Case 2 : $R \leq \|s_{i_0}s_i\| < \sqrt{2}\,R$.

Let (u_{P_1}, θ_{P_1}) be the point connecting ρ_i^1 and ρ_i^2, and (u_{P_2}, θ_{P_2}) be the point connecting ρ_i^2 and ρ_i^3. According to the construction of ρ_i^1, ρ_i^2 and ρ_i^3, the tangent lines to C_{i_0} at P_1 and P_2 pass through s_i. At most two tangent lines to C_{i_0} pass through s_i, thus P_1 and P_2 are the only points of C_{i_0} where $\gamma = \frac{\pi}{2}$ $[\pi]$. Therefore, the lines $\theta = u \pm \frac{\pi}{2}$ properly intersect neither ρ_i^{k-} nor ρ_i^{k+} $(k = 1, 2, 3)$. At last, the points $(\theta_1, \theta_1 - \frac{\pi}{2})$, $(\theta_2, \theta_2 + \frac{\pi}{2})$ and $(\theta_3, \theta_3 - \frac{\pi}{2})$ of $\mathcal{C}_{i_0}$ clearly belong to the relative interior of $\mathcal{Z}_i^1$, $\mathcal{Z}_i^2$ and $\mathcal{Z}_i^3$ respectively. □

4.3 Construction of $\delta(\mathcal{F}) \cap C_{i_0}$

We have seen in section 4.1 that the contribution of a circle C_{i_0} to $\delta(\mathcal{F})$ is given by the computation of $\cup_{i \neq i_0} \mathcal{Z}_i$ and $\cup_i \mathcal{Z}_i$. Propositions 14 and 16 show that the set of regions $\mathcal{Z}_i$ can be split into two subsets Ω_1 and Ω_2 as follows. As we know, a region $\mathcal{Z}_i$ (or $\mathcal{Z}_i^k$) is the region below ρ_i^+ (or ρ_i^{k+}) and above ρ_i^- (or ρ_i^{k-}). For convenience, if not specified, $\mathcal{Z}_i$ (resp. ρ_i) will denote either $\mathcal{Z}_i$ or $\mathcal{Z}_i^k$ (resp. ρ_i or ρ_i^k). Ω_1 (resp. Ω_2) is the set of regions $\mathcal{Z}_i$, $i \neq i_0$, such that the line $\theta = u + \frac{\pi}{2}$ (resp. $\theta = u - \frac{\pi}{2}$) intersects $\mathcal{Z}_i$ but neither ρ_i^+ nor ρ_i^-. By Propositions 14 and 16, the lines $\theta = u \pm \frac{\pi}{2}$ do not properly intersect the curves ρ_i. Thus, for $\mathcal{Z}_i \in \Omega_1$, we

can consider the curves ρ_i^+ in the domain $\{(u,\theta) \in S^1 \times [u+\frac{\pi}{2}, u+\frac{3\pi}{2}]\}$ and the curves ρ_i^- in $\{(u,\theta) \in S^1 \times [u-\frac{\pi}{2}, u+\frac{\pi}{2}]\}$. The union of the $\mathcal{Z}_i \in \Omega_1$ is therefore computed as the region that lies below the upper envelope of the ρ_i^+ and above the lower envelope of the ρ_i^-. We compute similarly the union of the regions of Ω_2.

Let us analyze the complexity of the above construction. The k_{i_0} helicoidal volumes $\mathcal{H}_i$ that intersect $\mathcal{C}_{i_0}$ can be found in $O(k_{i_0})$ amortized time once the Delaunay triangulation of the footholds has been computed which can be done in $O(n \log n)$ time [DD90, Tur91]. Since two curves ρ_i and ρ_j intersect each other at most once (Propositions 12, 13, 15) the upper and lower envelopes can be computed in $O(k_{i_0} \log k_{i_0})$ time and $O(k_{i_0}\alpha(k_{i_0}))$ space where α is the pseudo inverse of the Ackerman's function [Her89]. The union of Ω_1 and Ω_2 can be done in $O(k_{i_0}\alpha(k_{i_0}))$ time because each envelope is the graph of a function of u and two arcs of the two envelopes intersect each other at most once. At this time, we have computed $\cup_{i \neq i_0} \mathcal{Z}_i$.

The computation of $\cup_{i \neq i_0} \mathcal{Z}_i \cup \mathcal{Z}_{i_0}$ can be done as follows. Let $\rho_{i_0}^+$ and $\rho_{i_0}^-$ denote the upper and lower edges of $\mathcal{Z}_{i_0}$. As already observed, $\rho_{i_0}^+$ and $\rho_{i_0}^-$ are the line $\theta = u$ and $\theta = u - \pi$ (see Figure 7). We add to set Ω_2 the region $\mathcal{Z}_{i_0}$. The computation of $\cup_i \mathcal{Z}_i$ can be performed, as described above, within the same time and space bounds because Proposition 12 holds if only one of the two considered curved edges is a graph of a function of θ defined over a θ-interval smaller than π.

According to Theorem 6, Remark 7 and Section 4.1, the contribution of C_{i_0} to the interior of $\mathcal{F}$ is $int(compl(p_{//\theta}(compl(\cup_{i \neq i_0} \mathcal{Z}_i))))$, that is the interior of the projection onto C_{i_0} of the largest vertical strip Σ'_{i_0} included in $\cup_{i \neq i_0} \mathcal{Z}_i$. This projection is easily computed because the curved edges of $\cup_{i \neq i_0} \mathcal{Z}_i$ are monotone with respect to u (see Figures 6, 8). The computation of the contribution of C_{i_0} to the closure of $\mathcal{F}$, $compl(p_{//\theta}(compl(\cup_i \mathcal{Z}_i)))$, is done similarly by projecting the strip Σ_{i_0}. These computations yield the contribution of C_{i_0} to $\delta(\mathcal{F})$. Clearly, this step can be done in $O(k_{i_0} \log k_{i_0})$ time.

Moreover we label an arc of $\delta(\mathcal{F})$ either by i if the arc belongs to the circle C_i or by (i,j) if the arc belongs to the straight line segment $[s_i, s_j]$. The labels of the edges of $\delta(\mathcal{F})$ incident to C_{i_0} can be found as follows, without increasing the complexity. An arc of $\delta(\mathcal{F}) \cap C_{i_0}$ corresponds to a vertical strip $\Sigma_{i_0} \setminus \Sigma'_{i_0}$. An endpoint P of an arc is either the projection of a vertical edge of the strip or the projection of a point of intersection between two curved edges. In the first case, P is the intersection of C_{i_0} with some C_i and in the second case, P is the intersection of C_{i_0} with some line segment $[s_i, s_j]$. Hence, the labels of the edges of $\delta(\mathcal{F})$ incident to C_{i_0} can be found at no extra-cost during the construction.

Since $\mathcal{A}$ is the arrangement of the circles of radius R centered at the footholds, $\sum_{i_0=1}^{n} k_{i_0} = |\mathcal{A}|$. The above considerations yield the following theorem:

Theorem 17 *We can compute $\delta(\mathcal{F}) \cap \mathcal{A}$ and the labels of the edges of $\delta(\mathcal{F})$ incident to the arcs of $\delta(\mathcal{F}) \cap \mathcal{A}$ in $O(|\mathcal{A}| \log n)$ time and $O(|\mathcal{A}|\alpha(n))$ space.*

4.4 Computation of the arcs of $\delta(\mathcal{F})$ issued from a foothold

The previous section has shown how to compute all the vertices of $\mathcal{F}$ that are incident to at least one circular arc. It remains to find the vertices of $\mathcal{F}$ incident to two straight edges. As we have seen in Section 2, for any cell Γ of $\mathcal{A}$, the convex hull of the footholds reachable from any point of Γ coincides with $\mathcal{F} \cap \Gamma$. Therefore, a vertex of $\mathcal{F}$ incident to two straight edges of $\delta(\mathcal{F})$ is a foothold. Furthermore, considering a foothold s_{i_0} in a cell Γ of $\mathcal{A}$, s_{i_0} is a vertex of $\mathcal{F}$ incidents to two straight edges $\delta(\mathcal{F})$ if and only if s_{i_0} is a vertex of the convex hull of the footholds reachable from s_{i_0}. The k'_{i_0} footholds contained in the disk $D(s_{i_0}, R)$ can be found in $O(k'_{i_0})$ amortized time because we have already computed the Delaunay triangulation of the footholds [DD90, Tur91]. Thus, we can decide if s_{i_0} is a vertex of the convex hull of these k'_{i_0} footholds in $O(k'_{i_0})$ time and space. When s_{i_0} is a vertex of the convex hull, we can also find the two edges of the convex hull adjacent to s_{i_0} in $O(k'_{i_0})$ time and space. As the sum of the k'_i for $i \in \{1, \ldots, n\}$ is bounded by the size of $\mathcal{A}$, we obtain the following theorem:

Theorem 18 *The footholds belonging to $\delta(\mathcal{F})$ and the labels of the arcs of $\delta(\mathcal{F})$ issued from these footholds can be found in $O(|\mathcal{A}|)$ time and space.*

4.5 Construction of $\mathcal{F}$

Theorem 19 *The free space of the spider robot can be computed in $O(|\mathcal{A}| \log n)$ time and $O(|\mathcal{A}|\alpha(n))$ space.*

Proof: By Theorem 17, we have computed all the circular arcs of $\delta(\mathcal{F})$ and the labels of the edges of $\delta(\mathcal{F})$ incident to them. By Theorem 18, we have computed all the vertices of $\delta(\mathcal{F})$ that are incident to two straight edges of $\delta(\mathcal{F})$ and the label of these two edges. It remains to sort the vertices of $\delta(\mathcal{F})$ that appear on the line segments (s_i, s_j). We only consider the line segments (s_i, s_j) such that the corresponding label (i, j) appears during previous computations. Then, we sort the vertices of $\delta(\mathcal{F})$ that belong to each such relevant line. Since $|\delta(\mathcal{F})| = \Theta(|\mathcal{A}|)$ [BDDP95], all these sorting

can be done in $O(|\mathcal{A}| \log n)$ time. It is then an easy task to deduce a complete description of $\delta(\mathcal{F})$. □

5 Generalization to polygonal foothold regions

5.1 Introduction and preliminaries

We consider now the case where the set of footholds is no longer a set of points but a set $\mathcal{S}$ of pairwise disjoint polygonal regions bounded by n line segments $e_1, \ldots, e_n$. Clearly, $\mathcal{S}$ is a subset of the free space $\mathcal{F}$ of the spider robot. Let $\mathcal{F}_e$ denote the free space of the spider robot using as foothold regions only the edges $e_1, \ldots, e_n$. Suppose that the spider robot admits a stable placement outside $\mathcal{S}$ with its feet inside some polygonal footholds; then the placement remains stable if it retracts its legs on the boundary of these polygonal regions. Hence, $\mathcal{F} = \mathcal{F}_e \cup \mathcal{S}$. We show how to compute $\mathcal{F}_e$.

As observed in Remark 9, all we have done in Section 3 remains true if the foothold regions are line segments provided that $\mathcal{H}_i$ is replaced by $\mathcal{H}_{e_i}$ the generalized helicoidal volume defined by (see Figure 13):

$$\mathcal{H}_{e_i} = \{(P, \theta) \in I\!R^2 \times S^1 \,/\, P \in HD(s, \theta),\ s \in e_i\}.$$

The helicoidal volume associated to a point site s_i will be, up to the end, denoted by $\mathcal{H}_{s_i}$.

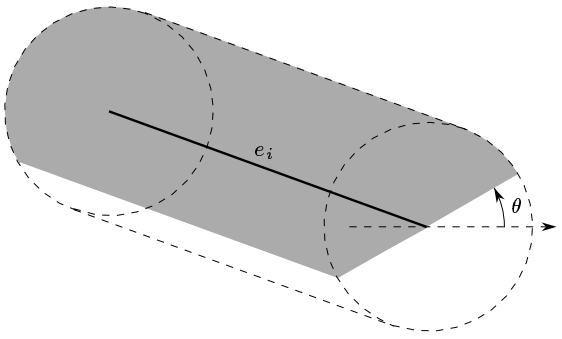

Figure 13: Section of $\mathcal{H}_{e_i}$ by the "plane" Π_θ.

Similarly, we define the generalized circle C_{e_i} as the set of points at distance R from e_i. Let $\mathcal{A}_e$ denote the arrangement of the n generalized circles $C_{e_1}, \ldots, C_{e_n}$. Notice that $|\mathcal{A}_e| = \Theta(n^2)$.

Each arc of the boundary $\delta(\mathcal{F}_e)$ of $\mathcal{F}_e$ is either an arc of C_{e_i}, corresponding to a maximal extension of one leg, or an arc corresponding to placements at the limit of stability of the spider robot. Similarly to what we did in Section 4, we compute first the contribution of each C_{e_i} to $\delta(\mathcal{F}_e)$ (Sections 5.2). Thereafter, we compute the arcs of $\delta(\mathcal{F}_e)$ that correspond to placements where the spider robot is at the limit of stability (Section 5.3). At last, we show how to construct $\mathcal{F}_e$ (and $\mathcal{F}$) in Section 5.4.

5.2 Computation of $\delta(\mathcal{F}_e) \cap \mathcal{A}_e$

We compute the contribution to $\delta(\mathcal{F}_e)$ of each generalized circles C_{e_i} in turn. We consider the contribution of $C_{e_{i_0}}$ to $\delta(\mathcal{F}_e)$ for some $i_0 \in \{1, \ldots, n\}$. $C_{e_{i_0}}$ is composed of two half circles and two straight line segments. In order to compute the contribution of $C_{e_{i_0}}$ to $\delta(\mathcal{F}_e)$, we evaluate first the contribution of the half circles and then the contribution of the straight line segments. For convenience, we will not compute the contribution of the half circles to $\delta(\mathcal{F}_e)$ but the contribution of the whole circles. Similarly, we will compute the contribution of the whole straight lines supporting the line segments of $C_{e_{i_0}}$.

Let s_{i_0} and s'_{i_0} denote the two endpoints of the line segment e_{i_0}, and let $C_{s_{i_0}}$ and $C_{s'_{i_0}}$ denote the unit circles centered at s_{i_0} and s'_{i_0} respectively. Let l_{i_0} and l'_{i_0} denote the two straight line segments of $C_{e_{i_0}}$, and L_{i_0} and L'_{i_0} their supporting lines. We show how to compute the contributions of $C_{s_{i_0}}$ and L_{i_0} to $\delta(\mathcal{F}_e)$; the contributions of $C_{s'_{i_0}}$ and L'_{i_0} can be computed likewise.

Let $\mathcal{C}_{s_{i_0}} = C_{s_{i_0}} \times S^1$ and $\mathcal{L}_{i_0} = L_{i_0} \times S^1$. Basically, we compute $\delta(\mathcal{F}_e) \cap C_{s_{i_0}}$ and $\delta(\mathcal{F}_e) \cap L_{i_0}$, as explained in Section 4.1, by computing $\cup_i(\mathcal{H}_{e_i} \cap \mathcal{C}_{s_{i_0}})$, $\cup_{i \neq i_0}(\mathcal{H}_{e_i} \cap \mathcal{C}_{s_{i_0}})$, $\cup_i(\mathcal{H}_{e_i} \cap \mathcal{L}_{i_0})$ and $\cup_{i \neq i_0}(\mathcal{H}_{e_i} \cap \mathcal{L}_{i_0})$. The properties of the new regions $\mathcal{Z}_{e_i} = \mathcal{H}_{e_i} \cap \mathcal{C}_{s_{i_0}}$ and $\mathcal{Y}_{e_i} = \mathcal{H}_{e_i} \cap \mathcal{L}_{i_0}$ are different though similar to the properties of $\mathcal{Z}_{s_i} = \mathcal{H}_{s_i} \cap \mathcal{C}_{s_{i_0}}$ described in Section 4.2. The analysis of $\mathcal{Z}_{e_i}$ and $\mathcal{Y}_{e_i}$ are subdivided into two parts: first, we consider the line D_i supporting e_i and we examine the regions $\mathcal{Z}_{D_i} = \mathcal{H}_{D_i} \cap \mathcal{C}_{s_{i_0}}$ and $\mathcal{Y}_{D_i} = \mathcal{H}_{D_i} \cap \mathcal{L}_{i_0}$ where $\mathcal{H}_{D_i}$ is the generalized helicoidal volume induced by D_i:

$$\mathcal{H}_{D_i} = \{(P, \theta) \in \mathbb{R}^2 \times S^1 \;/\; P \in HD(s, \theta),\ s \in D_i\}.$$

Then, we deduce $\mathcal{Z}_{e_i}$ (resp. $\mathcal{Y}_{e_i}$) from $\mathcal{Z}_{D_i}$, $\mathcal{Z}_{s_i}$ and $\mathcal{Z}_{s'_i}$ (resp. $\mathcal{Y}_{D_i}$, $\mathcal{Y}_{s_i} = \mathcal{H}_{s_i} \cap \mathcal{L}_{i_0}$ and $\mathcal{Y}_{s'_i}$) where s_i and s'_i are the two endpoints of e_i. Thereafter, we compute the

contribution of $C_{e_{i_0}}$ to $\delta(\mathcal{F}_e)$ in a way similar to what we did in Section 4.3. The following theorem sums up these results :

Theorem 20 *We can compute $\delta(\mathcal{F}_e) \cap \mathcal{A}_e$ and the labels of the edges of $\delta(\mathcal{F}_e)$ incident to the arcs of $\delta(\mathcal{F}_e) \cap \mathcal{A}_e$ in $O(|\mathcal{A}_e|\alpha_7(n)\log n)$ time and $O(|\mathcal{A}_e|\alpha_8(n))$ space.*

The proof of this theorem is detailed in Appendix A.

5.3 Arcs of $\delta(\mathcal{F}_e)$ corresponding to the placements where the spider robot is at the limit of stability

We now have to compute the edges of $\mathcal{F}_e$ that do not belong to $\mathcal{A}_e$. The arcs of $\delta(\mathcal{F}_e) \cap \mathcal{A}_e$ correspond to placements at the limit of accessibility of the spider robot, and reciprocally. Thus, other edges of $\mathcal{F}_e$ correspond to placements at the limit of stability of the spider robot. We denote by $\mathcal{S}_e$ the set of those edges. A placement P of the spider robot is at the limit of stability if and only if there exists a closed half-disk of radius R centered at P that does not contain any foothold except at least two footholds located on the diameter of the half-disk such that P is between these footholds. Thus, the edges of $\mathcal{S}_e$ are supported by the curves drawn by the midpoint of a ladder of length $2R$ moving by translation and rotation such that the ladder touches the boundary of the foothold regions in two points but does not intersect the interior of the foothold regions. Thus, edges of $\mathcal{S}_e$ are supported by the projection (onto $\mathbb{R}^2$) of the edges of the boundary of the free space of the ladder moving by translation and rotation amidst the foothold regions considered as obstacles, i.e. the set of $(P, \theta) \in \mathbb{R}^2 \times S^1$ such that the ladder of length $2R$, which has its midpoint at P and makes an angle θ with the x-axis, does not collide with the interior of the foothold regions. According to [SS87], the edges of the boundary of the free space of the ladder can be computed in $O(|\mathcal{A}_e| \log n)$ time and $O(|\mathcal{A}_e|)$ space. Clearly, the projection (onto $\mathbb{R}^2$) of each edge can be computed in constant time. The intersections between the projected edges do not need to be computed. Thus, we can compute, in $O(|\mathcal{A}_e| \log n)$ time and $O(|\mathcal{A}_e|)$ space (using [SS87]), a set of curves in $\mathbb{R}^2$ that support the arcs of $\delta(\mathcal{F}_e)$ that correspond to placements at the limit of stability of the spider robot. However, it remains to compute the portions of these curves that belong to $\delta(\mathcal{F}_e)$.

We introduce first some definitions and notations. The *ladder* has length $2R$. The relative interior of an e_i is called a *wall*. An endpoint of an e_i is called a *corner* (when several walls share an endpoint, we define only one corner at that point). A *placement* of the ladder is a pair $(P, \theta) \in \mathbb{R}^2 \times S^1$ where P is the location of the midpoint of the ladder and θ is the angle between the x-axis and the ladder. A

free placement of the ladder is a placement where the relative interior of the ladder does not intersect the walls. A *placement of type corner-ladder* is a placement of the ladder such that the relative interior of the ladder touches a *corner*. A *placement of type wall-endpoint* is a placement of the ladder such that an endpoint of the ladder touches a *wall*. A *placement of type corner-endpoint* is a placement of the ladder such that an endpoint of the ladder touches a corner. We now define *k-contact placements* of the ladder.

A *1-contact placement* is a free placement of type corner-ladder or wall-endpoint. A *2-contact placement* is either the combination of two 1-contact placements or a free placement of type corner-endpoint. A 2-contact placement is said of type (corner-ladder, corner-ladder), (corner-ladder, wall-endpoint), (wall-endpoint, wall-endpoint), or (corner-endpoint), in accordance to the types of placements involved in the 2-contact placement. Given two walls (resp. a wall and a corner, two corners, one corner), the set of 2-contact placements induced by these two walls (resp. the wall and the corner, the two corners, the single corner) is called a *2-contact curve*. A *3-contact placement* is either the combination of a 1-contact placement, and a 2-contact placement, or is a free placement of type corner-endpoint such that the ladder at that placement is parallel and has no common point with a wall ending at the corner; that last type of 3-contact placement, denoted (corner-endpoint, //), is considered in order that, any 2-contact curve ends at a 3-contact placement. Notice that, reciprocally, any 3-contact placement is an endpoint of a 2-contact curve. The types of the 3-contact placements are naturally defined by (corner-ladder, corner-ladder, corner-ladder), (corner-endpoint, wall-endpoint)... A *k-contact placement*, $k > 3$, is the combination of p 1-contact placements, q 2-contact placements and r 3-contact placements such that $p + 2q + 3r = k$.

Now, we define a *2-contact tracing* as the projection onto $\mathbb{R}^2$ of a 2-contact curve. Similarly as above, we define the types of the 2-contact tracings. Notice that, to any point P of a given 2-contact tracing $\mathcal{K}$ corresponds a unique placement (P, θ) of the ladder. It follows that, to any point P of a 2-contact tracing $\mathcal{K}$ corresponds a unique pair (M, N) of points of contact between the ladder at (P, θ) and the walls (when P is an endpoint of $\mathcal{K}$, a 3-contact placement corresponds to P. However (M, N) is unique by continuity). Notice that M and N are equal when $\mathcal{K}$ is a 2-contact tracing of type corner-endpoint. The points M and N are called the *contact points corresponding to* $P \in \mathcal{K}$.

A 2-contact tracing is either a straight line segment, an arc of ellipse, an arc of conchoid or a circular arc. Indeed, a 2-contact tracing of type (corner-ladder, corner-ladder) is a straight line segment; a 2-contact tracing of type (corner-ladder,

wall-endpoint) is an arc of conchoid (see Appendix B); a 2-contact tracing of type (wall-endpoint, wall-endpoint) is an arc of ellipse; a 2-contact tracing of type (corner-endpoint) is a circular arc (see figures below). As we said before, we can compute all these 2-contact tracings in $O(|\mathcal{A}_e| \log n)$ time and $O(|\mathcal{A}_e|)$ space [SS87], it remains to compute the parts of these curves that belong to $\delta(\mathcal{F}_e)$.

We first show that only some portions of the 2-contact tracings correspond to positions at the limit of stability of the spider robot. These portions are called the relevant 2-contact tracings. Then, we prove that we do not have to take into consideration the intersections between the relative interior of relevant 2-contact tracings. We also show that, if a point A is an end-point of several relevant 2-contact tracings, only two of them can support edges of $\mathcal{S}_e$ in the neighborhood of A. Then, we compute a graph whose edges are relevant 2-contact tracings and where the degree of each node is at most two. Finally, given two vertices of $\delta(\mathcal{F}_e) \cap \mathcal{A}_e$ that are connected (along $\delta(\mathcal{F}_e)$) by arcs that correspond to placements at the limit of accessibility of the spider robot, we compute these arcs using the graph.

Asmentioned above, a placement P of the spider robot is at the limit of stability if and only if there exists a closed half-disk of radius R centered at P that does not contain any foothold except at least two footholds located on the diameter of the half-disk, one on each side of P, these footholds are called *cpntact points* at placement P. Thus, a point P of a 2-contact tracing $\mathcal{K}$ may be on an arc of $\delta(\mathcal{F}_e)$ that correspond to placements at the limit of accessibility of the spider robot only if P is between the two contact points corresponding to $P \in \mathcal{K}$. The portions of the 2-contact tracings for which that property holds are called the *relevant 2-contact tracings*. The other portions are called the *irrelevant 2-contact tracings*. We now show how to compute the relevant 2-contact tracings for each type of contact. (see Figure 14). Let $\mathcal{K}$ denote a 2-contact tracing, let $P \in \mathcal{K}$ and let M and N be the two contact points corresponding to $P \in \mathcal{K}$.

Type (corner-endpoint):
$\mathcal{K}$ is a circular arc, and M and N coincide with one endpoint of the ladder. Thus, all the 2-contact tracings of type (corner-endpoint) are wholly irrelevant.

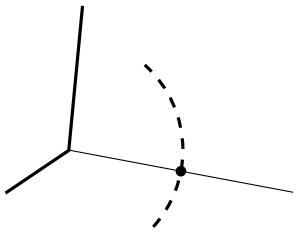

Type (wall-endpoint, wall-endpoint):
$\mathcal{K}$ is an arc of ellipse, M and N are the endpoints of the ladder and thus, P is between them. Thus, all the 2-contact tracings of type (wall-endpoint, wall-endpoint) are wholly relevant.

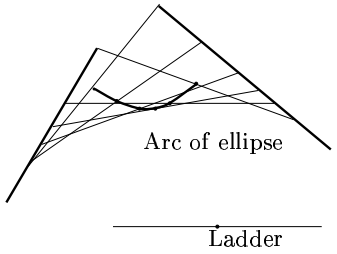

Type (corner-ladder, wall-endpoint):
$\mathcal{K}$ is an arc of conchoid. If the distance between the corner and the wall is greater than R, then, $\mathcal{K}$ is wholly relevant.

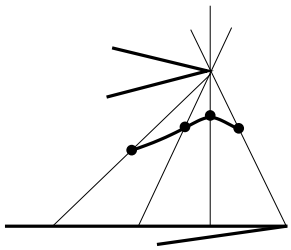

Otherwise, if that distance is smaller than R, then, the two relevant portions and the irrelevant portion of $\mathcal{K}$ are incident to the corner involved in the type of $\mathcal{K}$.

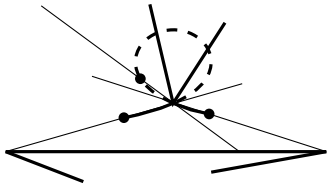

Notice that if the corner is an endpoint of the wall, then $\mathcal{K}$ degenerates in a line segment and the irrelevant portion of $\mathcal{K}$ is the portion which is not supported by the wall (see Figure 14).

Type (corner-ladder, corner-ladder):
$\mathcal{K}$ is a line segment. If the distance between the two corners is greater than R, then, $\mathcal{K}$ is wholly relevant; otherwise, the portion of $\mathcal{K}$ which is relevant is the line segment joining the two corners.

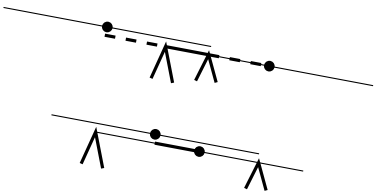

We show now that the intersections between the relative interiors of the relevant 2-contact tracings are not pertinent for the spider robot motion problem. We recall that, if a vertex A of $\delta(\mathcal{F}_e)$ belongs to $\mathcal{A}_e$, then we know by Theorem 20 the labels of the edges of $\delta(\mathcal{F}_e)$ incident to A. Otherwise, if $A \notin \mathcal{A}_e$, then the two edges of $\delta(\mathcal{F}_e)$ that end at A correspond to placements at the limit of stability of the spider robot.

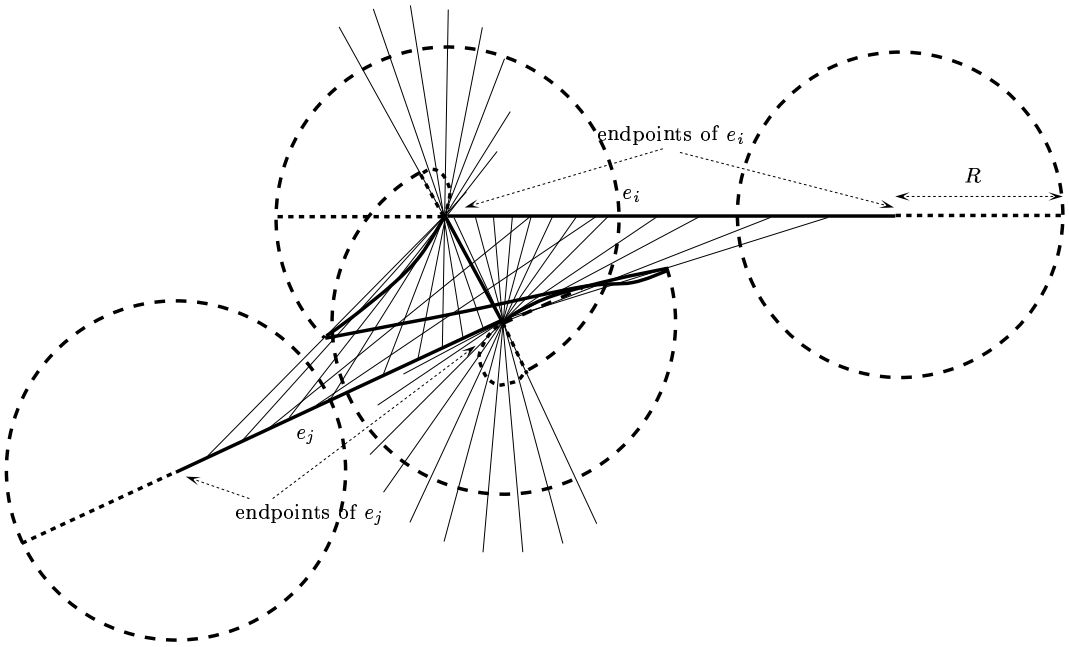

Figure 14: Relevant 2-contact tracings (thick curves) and irrelevant 2-contact tracings (dashed thick curves).

Proposition 21 *Any vertex A of $\delta(\mathcal{F}_e)$, such that $A \notin \mathcal{A}_e$, is an endpoint of the two relevant 2-contact tracings that support the edges of $\delta(\mathcal{F}_e)$ ending at A.*

Proof: Since the two edges of $\delta(\mathcal{F}_e)$ that end at A correspond to placements at the limit of stability of the spider robot, they are both supported by some relevant 2-contact tracings. Thus, we only have to prove that A is an endpoint of these two relevant 2-contact tracings.

Let $\mathcal{K}_1$ and $\mathcal{K}_2$ be these two relevant 2-contact tracings and assume for a contradiction that A is not an endpoint of $\mathcal{K}_1$ (nothing is assumed for A with respect to $\mathcal{K}_2$). Let $L_1 = (A, \theta_1)$ (resp. $L_2 = (A, \theta_2)$) be the placement of the ladder that correspond to $A \in \mathcal{K}_1$ (resp. $A \in \mathcal{K}_2$) and let M_1 and N_1 (resp. M_2 and N_2) be the corresponding contact points (see Figure 15). First, notice that $L_1 \neq L_2$. Indeed, otherwise, L_1 is at least a 3-contact placement and then, A must be an endpoint of $\mathcal{K}_1$, which contradicts our assumption.

By the definition of the relevant 2-contact tracings, A is between M_1 and N_1. Moreover, A cannot be equal to M_1 or N_1 since A is not an endpoint of $\mathcal{K}_1$. It follows that neither M_2 nor N_2 is equal to A, because otherwise L_1 would be a 3-contact placement. Therefore A is strictly between M_1 and N_1, and strictly between M_2 and N_2. Thus, A is strictly inside the polygon $(M_1M_2N_1N_2)$.

On the other hand, since A does not belong to any C_{e_i}, the walls supporting M_1, N_1, M_2 and N_2 intersect the open disk D_A of radius R centered at A. Thus, there exists four points M_1', N_1', M_2' and N_2' on these walls and in D_A, that are close enough to M_1, N_1, M_2 and N_2 respectively to ensure that A belongs to the interior of the polygon $(M_1'M_2'N_1'N_2')$. Since the distances from A to M_1', N_1', M_1' and N_2', are strictly smaller than R, A belongs to the interior of $\mathcal{F}_e$. This contradicts our assumption that A is a vertex of $\delta(\mathcal{F}_e)$ and yields the result. □

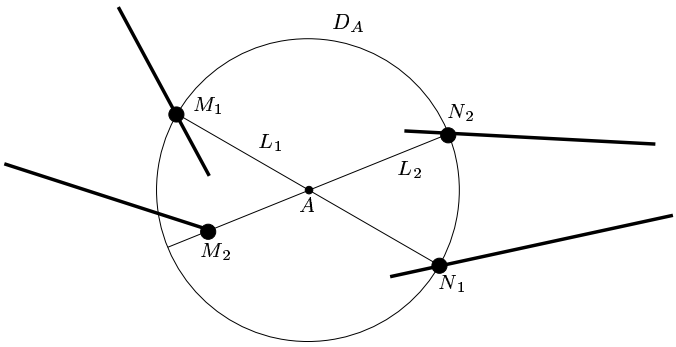

Figure 15: For the proof of Proposition 21.

Consider now the adjacency graph $\mathcal{G}$ of the relevant 2-contact tracings such that two relevant 2-contact tracing are connected in $\mathcal{G}$ if and only if they have a common endpoint (the intersections between the relative interior of the relevant 2-contact tracings are not considered). Notice that, given the set of relevant 2-contact tracings, $\mathcal{G}$ can simply be computed in $O(|\mathcal{A}_e| \log n)$ time. Now, given two vertices of $\delta(\mathcal{F}_e) \cap \mathcal{A}_e$ that can be joined by arcs of $\mathcal{S}_e$, we want to be able to compute these arcs. For computing these arcs, we cannot simply use the graph $\mathcal{G}$ because the degree of some nodes of $\mathcal{G}$ may be arbitrary large (see Figure 16). We show in the next proposition that we can deduce from $\mathcal{G}$ a graph $\mathcal{G}'$ such that the degree of each node of $\mathcal{G}'$ is at most two and that $\mathcal{G}'$ supports any portion of $\delta(\mathcal{F}_e)$ which is the concatenation of arcs of $\mathcal{S}_e \cap \mathcal{A}_e$.

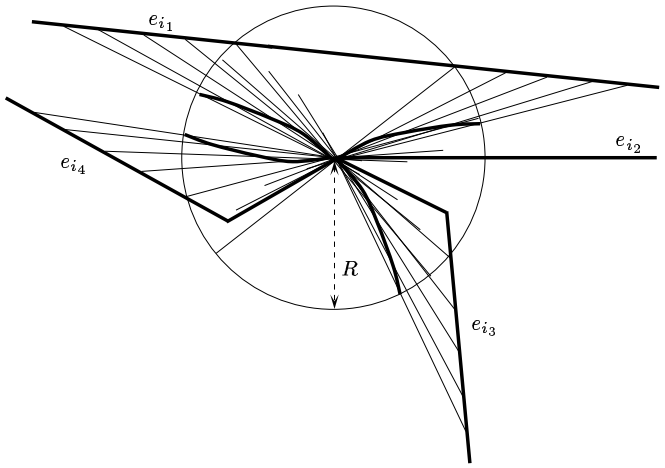

Figure 16: An arbitrary number of relevant 2-contact tracings that have a common endpoint.

We consider four hypotheses (H1,...,H4) that avoid to consider degenerate cases. They are not essential but substantially simplify the proof of the following proposition. In order to ensure that the degree of each vertex of the free space of the ladder is three, we make the three hypotheses H1, H2 and H3.

H1 The line segments $e_1, \ldots, e_n$ compose the boundary of a set of non degenerated polygons (i.e. no polygon is reduced to a line segment or to a point).

H2 The ladder does not admit any 4-contact placement.

H3 The arc of conchoid drawn by an endpoint of the ladder when its other endpoint moves along a wall while the ladder remains in contact with a corner, is not tangent to any other wall. According to Lemma 48 this hypothesis avoids only degenerate cases.

H4 The ladder does not admit any 3-contact placement when its midpoint is located at a corner.

Proposition 22 *For any node A of $\mathcal{G}$ of degree k such that $A \notin \mathcal{A}_e$, at most two relevant 2-contact tracings can support $\delta(\mathcal{F}_e)$ in a sufficiently small neighborhood of A. Moreover, we can determine these at most two curves in $O(k \log k)$ time and $O(k)$ space.*

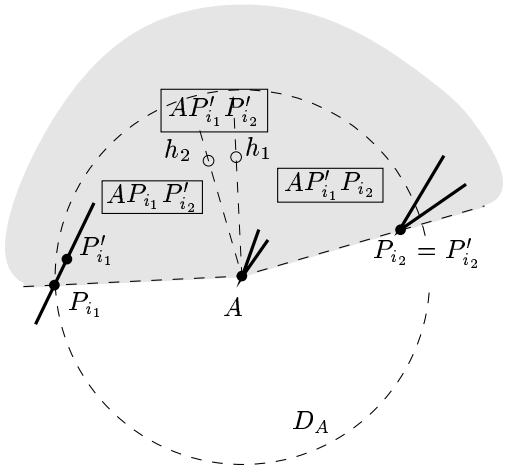

Figure 17: Wedge $P_{i_1}AP_{i_2}$ is in $\mathcal{F}_e$ near A.

Proof: Let $A \notin \mathcal{A}_e$ a node of $\mathcal{G}$ of degree k, D_A is the open disk of radius R centered at A. We will distinguish two cases: A is or is not a corner.

A is a corner.

Let $\mathcal{K}_1, \ldots, \mathcal{K}_k$ be the relevant 2-contact tracings that end at A, and let $L_i = (A, \phi_i)$ be the placement of the ladder that corresponds to $A \in \mathcal{K}_i$. We assume that $k > 2$, otherwise Proposition 22 is trivial.

The 2-contact tracing $\mathcal{K}_i$ has to involve a least a different contact from the corner-ladder contact in A; if this contact is a corner-ladder contact we define $P_i = P'_i$ as the corner ($\neq A$) defining this contact (notice that $P_i = P'_i \in D_A$ by Hypothesis H4); if this contact is a wall-endpoint contact we define P_i as the contact point between this wall and the ladder at placement L_i, since $A \notin \mathcal{A}_e$, the wall must intersect D_A and we define P'_i as a point in that intersection in a neighborhood of P_i.

Fact: $\forall i \neq j, \ \ \phi_i \neq \phi_j$,
otherwise, placement $L_i = L_j$ is a 3-contact with midpoint on a corner contradicting Hypothesis H4.

Fact: *A is a non-flat vertex of $CH(A, P_1, \ldots, P_k)$ or belongs to the interior of $\mathcal{F}_e$.* Assume that $A \in \delta(\mathcal{F}_e)$. Then, A lies on the boundary of $\mathrm{CH}(A, P_1, \ldots, P_k)$ because, otherwise, the P'_i provide footholds such that the spider robot can move in a neighborhood of A. Furthermore, A must be a non-flat vertex of $\mathrm{CH}(A, P_1, \ldots, P_k)$, by Hypothesis H4.

Assume that A does not belong to the interior of $\mathcal{F}_e$, and let P_{i_1} and P_{i_2} be the two vertices of $\mathrm{CH}(A, P_1, \ldots, P_k)$ such that P_{i_1}, A and P_{i_2} are consecutive along the boundary of $\mathrm{CH}(A, P_1, \ldots, P_k)$. We will exhibit a stable placement for the spider robot at any position P inside the intersection of the wedge $P_{i_1}AP_{i_2}$ and a neighborhood of A. Let h_1 and h_2 be two points in the wedge $P_{i_1}AP_{i_2}$ such that the wedges $P_{i_1}Ah_1$ and $h_2AP_{i_2}$ have angle $\frac{\pi}{2}$.
— If P is in the wedge $P_{i_1}Ah_2$, and is close enough to A, the footholds A, P_{i_1} and P'_{i_2} yield a stable placement for the spider robot (see Figure 17).
— If P is in the wedge h_2Ah_1, and is close enough to A, footholds A, P'_{i_1} and $P'i_2$ yield a stable placement for the spider robot.
— If P is in the wedge $h_1AP_{i_1}$, and is close enough to A, footholds A, P'_{i_1} and Pi_2 yields a stable placement for the spider robot.

Fact: *$\mathcal{K}_i$, $i \notin \{i_1, i_2\}$, cannot support an edge of $\delta(\mathcal{F}_e)$ incident to A.*
We assume that A is a non-flat vertex of $\mathrm{CH}(A, P_1, \ldots, P_k)$ because, otherwise, A belongs to the interior of $\mathcal{F}_e$ and the claim is obvious. A 2-contact tracing $\mathcal{K}_i$, $i \notin \{i_1, i_2\}$, cannot be an arc of ellipse because, otherwise, L_i is a 3-contact placement contradicting Hypothesis H4. Thus, $\mathcal{K}_i$ can be either the segment AP_i or an arc of conchoid which is tangent to the segment AP_i at A by Lemma 47. The point P_i strictly belongs to the wedge $P_{i_1}AP_{i_2}$, because we have shown that $\phi_i \notin \{\phi_{i_1}, \phi_{i_2}\}$. Thus, $\mathcal{K}_i$ is strictly inside the wedge $P_{i_1}AP_{i_2}$ and thus inside $\mathcal{F}_e$, in a neighborhood of A. Therefore, $\mathcal{K}_i$ cannot support $\delta(\mathcal{F}_e)$, in a neighborhood of A.

Hence, by sorting the P_i in polar order around A, we can determine, in $O(k \log k)$ time, if A is a non-flat vertex of $\mathrm{CH}(A, P_1, \ldots, P_k)$, and if so, determine i_1 and i_2. If A is a non-flat vertex of $\mathrm{CH}(A, P_1, \ldots, P_k)$, then, only $\mathcal{K}_{i_1}$ and $\mathcal{K}_{i_2}$ can support an edge of $\delta(\mathcal{F}_e)$ incident to A. Otherwise, A belongs to the interior of $\mathcal{F}_e$ and none of the 2-contact tracings $\mathcal{K}_1, \ldots, \mathcal{K}_k$ can support an edge of $\delta(\mathcal{F}_e)$ incident to A.

A is not a corner.

Fact: *There is only one relevant placement L with center in A.*
Indeed, either A is in a wall, and the only possible orientation for the ladder is the orientation of the wall, or A is not a foothold, and thus, if there is two distinct relevant 2-contact placements at A, there exists four contact points P_1, P_2, P_3, P_4 such that $|AP_i| \leq R$ and that the interior of $\mathrm{CH}(P_1, P_2, P_3, P_4)$ contains A. Since $A \notin \mathcal{A}_e$, there exists four footholds P'_1, P'_2, P'_3, P'_4 in D_A and in some neighborhoods of P_1, P_2, P_3, P_4, respectively, such that A belongs to the interior of $\mathrm{CH}(P'_1, P'_2, P'_3, P'_4)$. Thus, $A \notin \delta(\mathcal{F}_e)$ which contradicts our assumption.

Fact: *There are at most six 2-contact tracings incident to A.*
Since the general position hypothesis H2 forbid k-contacts for $k > 3$, A corresponds

to a 3-contact placement. The three possible choices of two contacts among three gives three 2-contact tracing intersecting in A and thus, six arcs incident to A.

Fact: *There are three 2-contact tracings incident to A.*
If the 3-contact placement L is of type (corner-endpoint, //), then there are only three 2-contact tracings incident to A, that are two circular arcs and one line segment. Otherwise, it comes from the general position hypotheses H1, H2 and H3 (designed to ensure that property) that a 2-contact tracing cannot be valid on both side of the 3-contact, i.e. on one side of the 3-contact placement, the placements are not free. We detail below that proof.

Fact: *There are two relevant 2-contact tracings incident to A.*
According to Hypothesis H4, at the 3-contact placement L, two contact points are on the same side of A. Thus, only two of the three 2-contact tracings incident to A are relevant.

Now, we prove that Hypotheses H1, H2 and H3 ensure that three 2-contact tracings are incident to A, by considering in turn each possible type of the 3-contact placement $L = (A, \phi)$.

Type (wall-endpoint, wall-endpoint, wall-endpoint):
This type of 3-contact placement cannot occur because the walls do not intersect each others since the polygonal foothold regions are pairwise disjoint, by assumption.

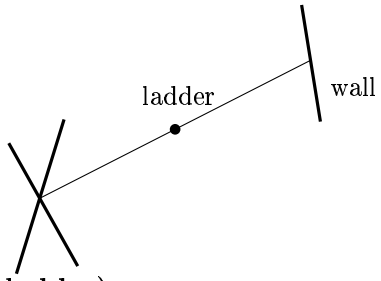

Type (corner-ladder, corner-ladder, corner-ladder):
This type of 3-contact placement does not appear because that contradicts Assumption H2, that says that there is no 4-contact placement.

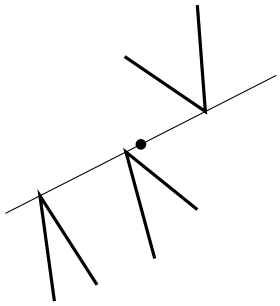

Type (corner-endpoint, //):
There are clearly three 2-contact tracings incident to A, that are two circular arcs and one line segment.

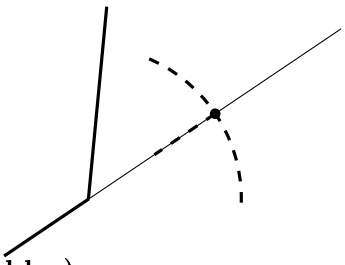

Type (wall-endpoint, corner-ladder, corner-ladder):
Let P_1 and P_2 denote the corners involved in the 3-contact placement, and let P_1' be the point of the ladder that coincide with P_1 when the ladder is at placement L. The wall and the ladder at L are not collinear by Hypothesis H2. Thus, translating the ladder in a direction parallel to P_1P_2 is possible in only one way if we forbid the ladder intersecting the wall. Thus, only one 2-contact tracing of type (corner-ladder, corner-ladder) ends at A.

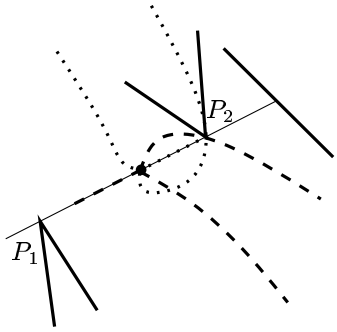

According to Lemma 47, the conchoid drawn by P_1' when the ladder moves keeping contact with P_2 and the wall, is not tangent to the ladder at placement L, and thus the ladder cannot move in both direction without intersecting one of the walls incident to P_1 (there is at least one wall incident to P_1 and not parallel to P_1P_2 by Hypothesis H1). Thus, only one 2-contact tracing of type (wall-endpoint, corner-ladder) involving P_1 ends at A. That result applies symmetrically to the 2-contact tracing involving P_2.

Type (wall-endpoint, wall-endpoint, corner-ladder):
We denote by P_0, e_{i_1} and e_{i_2} the corner and the two walls involved in the 3-contact placement.
According to Hypothesis H2, the two walls are not both parallel to the ladder at L.
If the ladder at L is collinear to one wall, then, by Hypotheses H1 and H2, there exists another wall non parallel to the ladder and incident to the corner. Then, there are three 2-contact tracings incident to A that are, a line segment, an arc of conchoid and an arc of ellipse.

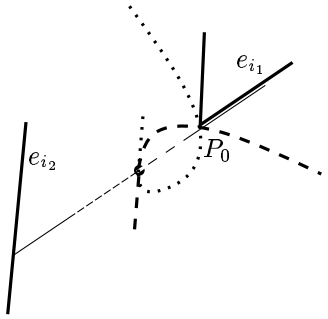

We now suppose that neither e_{i_1} nor e_{i_2} is parallel to the ladder at L. According to Hypothesis H3 (which has been designed especially for that case), the ladder at placement L can move only in one direction, remaining in contact with P_0 and e_{i_1} without intersecting e_{i_2}. Thus, only one 2-contact tracing of type (wall-endpoint, corner-ladder) involving e_{i_1} ends at A. Similarly, only one 2-contact tracing of type (wall-endpoint, corner-ladder) involving e_{i_2} ends at A.

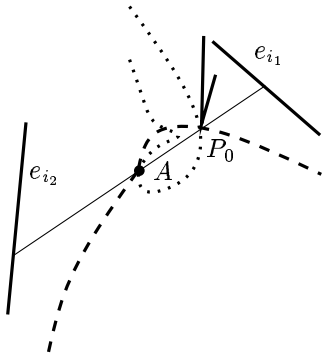

It remains to prove that only one arc of the ellipse drawn by the midpoint of the ladder keeping the contact with e_{i_1} and e_{i_2} is valid. If e_{i_1} and e_{i_2} are parallel, the ellipse degenerates to a line segment parallel to e_{i_1} (and to e_{i_2}) and only one arc of the ellipse, incidents to A, is valid. Now, we assume that e_{i_1} and e_{i_2} are not parallel. Let $\varepsilon > 0$ small enough and L' (resp. L'') be the placement of the ladder with orientation $\phi + \varepsilon$ (resp. $\phi - \varepsilon$) in contact with P_0 and e_{i_1}.

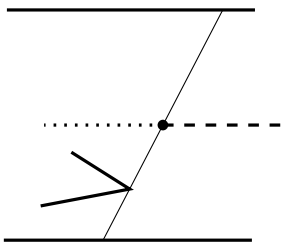

By Hypothesis H3, the ladder at either L' or L'' intersects e_{i_2}. Let t' (resp. t'') be the translation parallel to e_{i_1} that map the ladder at L' (resp. L'') to the position in contact with both e_{i_1} and e_{i_2}. The translations t' and t'' have opposite directions since exactly one of the ladder at L' and L'' intersects e_{i_2}. Thus, at most one of the ladder at $t'(L')$ and $t''(L'')$ is free, because one has to intersect a wall incident to P_0 (which exists and is not of direction ϕ by Hypothesis H1). Therefore, at most one of the two arcs of ellipse incident to A is a 2-contact tracing.

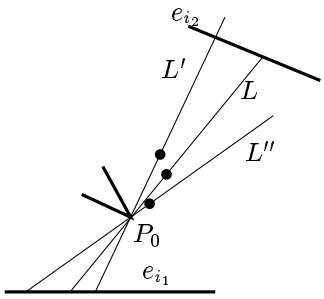

Type (corner-endpoint, corner-ladder):

Clearly, only three 2-contact tracings end at A that are either, a line segment, an arc of conchoid and a circular arc, or two arcs of conchoid and a circular arc.

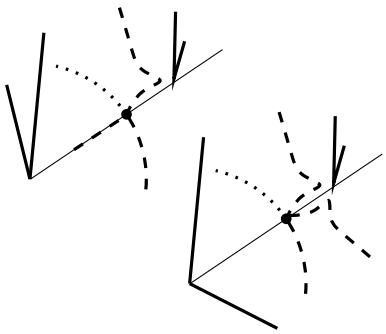

Type (corner-endpoint, wall-endpoint):
In this case, it is also clear that, three 2-contact tracings end at A, that are, a circular arc and, either an arc of conchoid and an arc of ellipse, or two arcs of ellipse.

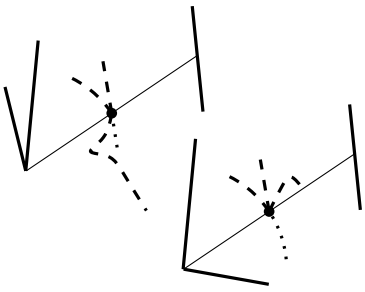

□

Now, consider the graph $\mathcal{G}$ and each node A in turn. If $A \in \mathcal{A}_e$, we disconnect all the edges of $\mathcal{G}$ that end at A. Notice that for each such node A, we know, by

Theorem 20, if $A \in \delta(\mathcal{F}_e)$ and, in such a case, the labels of the edges of $\delta(\mathcal{F}_e)$ incident to A. If $A \notin \mathcal{A}_e$, we disconnect the edges ending at A except those (at most two) that may support $\delta(\mathcal{F}_e)$ in a neighborhood of A (see Proposition 22). In this way, we obtain a graph $\mathcal{G}'$ such that the degree of each node is one or two. We consider each connected component of this new graph as a curve. Let Δ be this set of curves. We do not know if these curves are simple or not, but, in accordance with the graph $\mathcal{G}'$, they behaves like simple curves. Indeed, given any pair of points on a curve $\mathcal{K} \in \Delta$, there is one or two ways (depending if $\mathcal{K}$ is a closed curve or not) to connect them on $\mathcal{K}$ in accordance with the graph $\mathcal{G}'$. In the sequel, these curves are called *pseudo-simple*. Then, according to Propositions 21 and 22, we get the following theorem:

Theorem 23 *We can compute, in $O(|\mathcal{A}_e| \log n)$ time and $O(|\mathcal{A}_e|)$ space, a set Δ of pseudo-simple curves that support the edges of $\delta(\mathcal{F}_e)$ corresponding to placements at the limit of stability of the spider robot. Moreover, any portion $\mathcal{P}$ of $\delta(\mathcal{F}_e)$ either intersects $\mathcal{A}_e$ or belongs to a unique curve of Δ.*

5.4 Construction of $\mathcal{F}_e$ and $\mathcal{F}$

We can now construct $\mathcal{F}_e$ and $\mathcal{F}$. Let $\lambda_k(n)$ denote the maximum length of the Davenport-Schinzel sequence of order k on n symbols and $\alpha_k(n) = \lambda_k(n)/n$.

Theorem 24 *Given, as foothold regions, a set of n non intersecting straight line segments that satisfies Hypotheses H1, H2, H3 and H4, we can compute the free space $\mathcal{F}_e$ of the spider robot in $O(|\mathcal{A}_e|\alpha_8(n) \log n)$ time and $O(|\mathcal{A}_e|\alpha_8(n))$ space.*

Proof: By Theorem 20, we can compute the contribution of $\mathcal{A}_e$ to $\delta(\mathcal{F}_e)$ and the label of the edges of $\delta(\mathcal{F}_e)$ incident to them in $O(|\mathcal{A}_e|\alpha_7(n) \log n)$ time and $O(|\mathcal{A}_e|\alpha_8(n))$ space. By Theorem 23, we can compute, in $O(|\mathcal{A}_e| \log n)$ time and $O(|\mathcal{A}_e|)$ space, a set Δ of pseudo-simple curves that support the edges of $\delta(\mathcal{F}_e)$ that do not belong to $\mathcal{A}_e$. Moreover, any portion $\mathcal{P}$ of $\delta(\mathcal{F}_e)$ such that $\mathcal{P} \cap \mathcal{A}_e = \emptyset$ belongs to a unique curve of Δ. Thus, by sorting all the vertices of $\delta(\mathcal{F}_e) \cap \mathcal{A}_e \cap \Delta$ on the relevant curves of Δ, we obtain all the edges of $\delta(\mathcal{F}_e)$ that belong to a connected component of $\delta(\mathcal{F}_e)$ intersecting $\mathcal{A}_e$. Indeed, for each vertex $A \in \delta(\mathcal{F}_e) \cap \mathcal{A}_e \cap \Delta$, we know, in a neighborhood of A, the part of the curve of Δ that belongs to $\delta(\mathcal{F}_e)$ because we can simply determine, for each edge, a side of the edge that belongs to $\mathcal{F}_e$. Then, it is an easy task to deduce all the connected components of $\delta(\mathcal{F}_e)$ that intersect $\mathcal{A}_e$.

It remains to compute the connected components of $\delta(\mathcal{F}_e)$ that do not intersect $\mathcal{A}_e$. Each of these components must be a closed curve of Δ. Moreover, all the curves

of Δ belong to $\mathcal{F}_e$. Thus, according to Theorem 23, any closed curve $\mathcal{K}$ of Δ that does not intersect $\mathcal{A}_e$ is either a connected component of $\delta(\mathcal{F}_e)$ or is strictly included in $\mathcal{F}_e$. Therefore, by considering, in addition, all the closed curves of Δ that do not intersect $\mathcal{A}_e$, we finally obtain a set Ψ of closed curves that contains $\delta(\mathcal{F}_e)$ and such that any curve of Ψ is either a connected component of $\delta(\mathcal{F}_e)$ or is strictly included in $\mathcal{F}_e$.

At last, as we can simply determine, for each curve of Ψ, a side of the edge that belongs to $\mathcal{F}_e$, we can easily deduce from Ψ the free space $\mathcal{F}_e$. That concludes the proof since all these computations can be done in $O(|\mathcal{A}_e|\alpha_8(n)\log n)$ time and $O(|\mathcal{A}_e|\alpha_8(n))$ space. □

As we said at the beginning of Section 5, the free space of the spider robot using as foothold regions a set of polygonal regions is obtained by adding these polygonal regions to $\mathcal{F}_e$. This does not increase the geometric complexity of the free space nor the complexity of the computation. Thus, we get the following theorem:

Theorem 25 *Given a set of pairwise disjoint polygonal foothold regions with n edges in total that satisfies Hypotheses H1, H2, H3 and H4, we can compute the free space $\mathcal{F}$ of the spider robot in $O(|\mathcal{A}_e|\alpha_8(n)\log n)$ time and $O(|\mathcal{A}_e|\alpha_8(n))$ space.*

The function $\alpha_8(n)$ is extremely slowly growing and can be considered as a small constant in practical situations. This result is almost optimal since, as shown in [BDDP95], $\Omega(|\mathcal{A}_e|)$ is a lower bound for the size of $\mathcal{F}$.

6 Conclusion

We have seen in Theorem 19 that, when the foothold regions are n points in the plane, the free space of the spider robot can be computed in $O(|\mathcal{A}|\log n)$ time and $O(|\mathcal{A}|\alpha(n))$ space where $\alpha(n)$ is the pseudo inverse of the Ackerman's function and $\mathcal{A}$ the arrangement of the n circles of radius R centered at the footholds. By [BDDP95] the size of $\mathcal{F}$ is known to be $\Theta(|\mathcal{A}|)$. The size of $\mathcal{A}$ is $O(n^2)$ but, if k denotes the maximum number of disks of radius R centered at the footholds that can cover a point of the plane, it can be shown that $|\mathcal{A}| = O(kn)$ [Sha91]. Thus, in case of sparse footholds, the sizes of $\mathcal{A}$ and $\mathcal{F}$ are linearly related to the number of footholds. Moreover $|\mathcal{F}|$ is usually much smaller that $|\mathcal{A}|$, even when $\mathcal{A}$ has quadratic size.

When the foothold regions are n straight line segments or polygons with n edges in total, the free space of the spider robot can be computed in $O(|\mathcal{A}_e|\alpha_8(n)\log n)$ time and $O(|\mathcal{A}_e|\alpha_8(n))$ space. $n\alpha_k(n) = \lambda_k(n)$ is the maximum length of the Davenport-Schinzel sequence of order k on n symbols; $\mathcal{A}_e$ is the arrangement of the n curves

consisting of the points lying at distance R from the straight line edges. Notice that $\alpha(n) = \alpha_3(n)$ and also that the size of $\mathcal{A}_e$ is $O(n^2)$.

It should be observed that, in the case of point footholds, our algorithm implies that $O(|\mathcal{A}|\alpha(n))$ is an upper bound for $|\mathcal{F}|$. However, this bound is not tight since $|\mathcal{F}| = \Theta(|\mathcal{A}|)$ [BDDP95]. In the case of polygonal footholds, our analysis implies that $O(|\mathcal{A}_e|\alpha_8(n))$ is an upper bound of $|\mathcal{F}|$. We let as an open problem to close the (small) gap between this upper bound and the $\Omega(|\mathcal{A}_e|)$ lower bound.

Once the free space $\mathcal{F}$ is known, several questions can be answered. In particular, given two points in the same connected component of $\mathcal{F}$, the algorithm in [BDDP95] allows to compute a motion, i.e. a sequence of leg assignments that allow the robot to move from one point to the other.

A Proof of Theorem 20

We prove in this appendix the Theorem 20 stated in Section 5.2. We use the notations introduced in Section 5.2. To avoid confusion, the objects, C_i, $\mathcal{C}_i$, $\mathcal{H}_i$, $\mathcal{R}_i^{\pm}$, $\mathcal{Z}_i$, $\rho_i^{\pm}$, associated to a point site s_i are denoted by C_{s_i}, $\mathcal{C}_{s_i}$, $\mathcal{H}_{s_i}$, $\mathcal{R}_{s_i}^{\pm}$, $\mathcal{Z}_{s_i}$, $\rho_{s_i}^{\pm}$. We analyze the regions $\mathcal{Z}_{e_i}$ in Section A.1. We examine in Section A.2 the regions $int(\mathcal{H}_{e_i}) \cap \mathcal{C}_{s_{i_0}}$. Then, in Section A.3, we show how to compute the contribution to $\delta(\mathcal{F}_e)$ of all the circles (of radius R) centered at the endpoints of the e_i. At last, we study the regions $\mathcal{Y}_{e_i}$ and show how to compute the contribution of the line segments of the C_{e_i} to $\delta(\mathcal{F}_e)$, in Section A.4.

A.1 Properties of the $\mathcal{Z}_{e_i}$

We study here the regions $\mathcal{Z}_{e_i} = \mathcal{H}_{e_i} \cap \mathcal{C}_{s_{i_0}}$. We use for the torus $\mathcal{C}_{s_{i_0}}$ the vocabulary introduced in Section 4.2. As we said above, we study first the regions $\mathcal{Z}_{D_i} = \mathcal{H}_{D_i} \cap \mathcal{C}_{s_{i_0}}$. For convenience, we identify in the sequel the slope of a straight line D_i with the angle γ_i between the (oriented) x-axis and D_i; γ_i is defined modulo π. We assume, for the sake of simplicity, that the regions $\mathcal{Z}_{e_i}$ and $\mathcal{Z}_{D_i}$ under consideration are not reduced to the empty set.

Proposition 26 *If $s_{i_0} \notin D_i$, $\mathcal{Z}_{D_i}$ is a connected region bounded by two vertical line segments of length π, and two curved edges $\rho_{D_i}^+$ and $\rho_{D_i}^-$ which are symmetrical with respect to the lines $\theta = \gamma_i$ and $\theta = \gamma_i + \pi$ (see Figures 18 and 19).*

Proof: Since $s_{i_0} \notin D_i$, $\mathcal{Z}_{D_i}$ is bounded by two vertical line $u = u_1$ and $u = u_2$ where u_1 and u_2 are the parameters on the circle $C_{s_{i_0}}$ of the two points I_1 and I_2 at distance R from D_i (see Figure 20). Let s be a generic point of D_i and s_1 (resp. s_2) be the point of D_i at distance R from I_1 (resp. I_2). Let $\mathcal{Z}_s$ denote the intersection between the torus $\mathcal{C}_{s_{i_0}}$ and the helicoidal volume $\mathcal{H}_s$ associated to s.

$\mathcal{Z}_{D_i}$ is the union of the regions $\mathcal{Z}_s$, $s \in D_i$. As $\mathcal{Z}_s$ is connected (see Proposition 11) and continuous with respect to s, $\mathcal{Z}_{D_i}$ is connected.

For any $s \neq s_1$ (resp. $s \neq s_2$) the circle of radius R centered at s does not contain I_1 (resp. I_2), thus $\mathcal{Z}_{s_1}$ (resp. $\mathcal{Z}_{s_2}$) coincides with $\mathcal{Z}_{D_i}$ on the line $u = u_1$ (resp. $u = u_2$). Therefore, $\mathcal{Z}_{D_i}$ is a region bounded by two vertical line segments of length π (see Proposition 11).

The region $\mathcal{Z}_{D_i}$ is symmetrical with respect to the line $\theta = \gamma$ because the Minkowski's sum of $HD(O, \gamma_i + \theta)$ and D_i is equal to the Minkowski's sum of $HD(O, \gamma_i - \theta)$ and D_i. Since γ_i is defined modulo π, $\rho_{D_i}^+$ and $\rho_{D_i}^-$ are also symmetrical with respect to the line $\theta = \gamma_i + \pi$. □

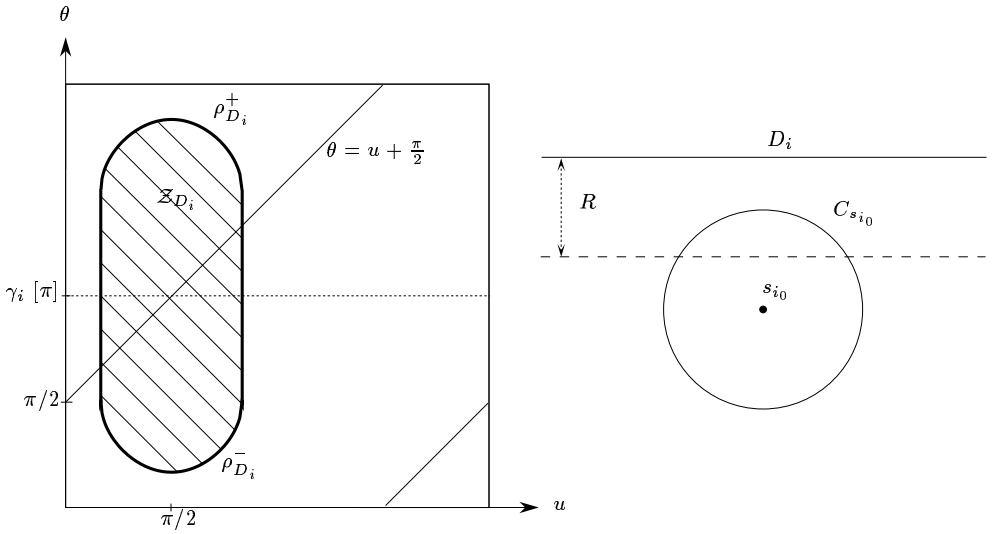

Figure 18: $\mathcal{Z}_{D_i}$ and the relative positions of $C_{s_{i_0}}$ and D_i that correspond.

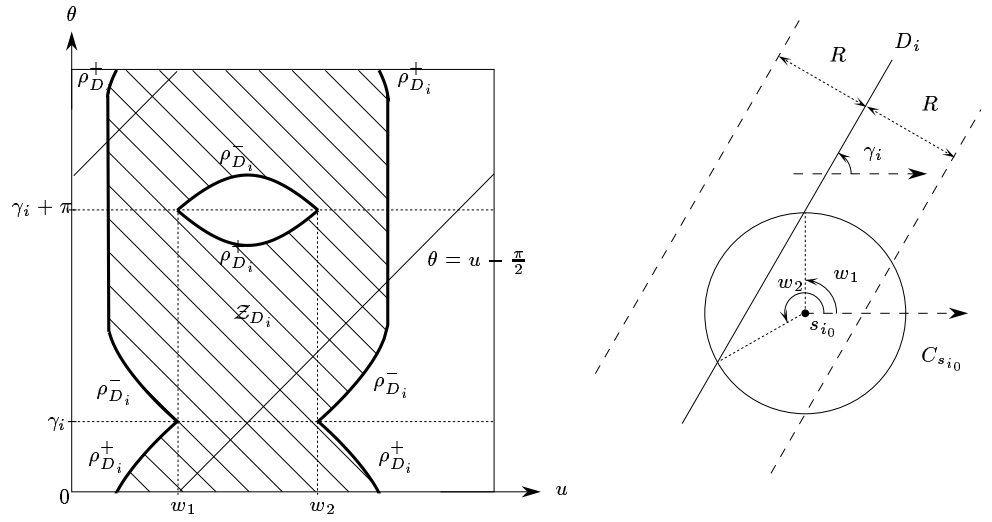

Figure 19: $\mathcal{Z}_{D_i}$ and the relative positions of $C_{s_{i_0}}$ and D_i that correspond.

Proposition 27 *If D_i does not intersect $C_{s_{i_0}}$, the line $\theta = u + \frac{\pi}{2}$ properly intersects the region $\mathcal{Z}_{D_i}$ but neither its upper nor its lower edges $\rho^+_{D_i}$ and $\rho^-_{D_i}$ (see Figure 18).*

Proof: We use here the notations of the previous proof.

Let I'_1 (resp. I'_2) denote the point of intersection distinct from I_1 (resp. I_2) between $C_{s_{i_0}}$ and the circle of radius R centered at s_1 (resp. s_2) (see Figure 20). Let u'_1 (resp. u'_2) be its parameter on $C_{s_{i_0}}$. By the definition of s_1 and I_1, the lines $(s_1 I_1)$ and D_i are orthogonal; therefore, $(s_{i_0} I'_1)$ and D_i are also orthogonal. The same argument shows that $(s_{i_0} I'_2)$ and D_i are orthogonal. It follows that $I'_1 = I'_2$ and $u'_1 = u'_2$.

On the other hand, since D_i does not intersect $C_{s_{i_0}}$, the angle $\angle(\overrightarrow{I_1 s_{i_0}}, \overrightarrow{I_1 s_1})$ is greater than $\pi/2$ and therefore $\|s_{i_0} s_1\| \geq \sqrt{2}\, R$. Similarly, $\|s_{i_0} s_2\| \geq \sqrt{2}\, R$. The region $\mathcal{Z}_{D_i}$ contains $\mathcal{Z}_{s_1}$ (resp. $\mathcal{Z}_{s_2}$) which contains the line $\theta = u + \frac{\pi}{2}$ for u in the interval $[u_1, u'_1]$ (resp. $[u'_2, u_2]$) (see Proposition 14). Since $u'_1 = u'_2$, $\mathcal{Z}_{D_i}$ contains the line $\theta = u + \frac{\pi}{2}$ for $u \in [u_1, u_2]$. Furthermore, for $u = u_1$ (resp. $u = u_2$) this line intersects the vertical edge of $\mathcal{Z}_{s_1}$ (resp. $\mathcal{Z}_{s_2}$) (see Proposition 14) which coincides with the vertical edge of $\mathcal{Z}_{D_i}$ (see the previous proof). □

Proposition 28 *If D_i intersects $C_{s_{i_0}}$ such that $s_{i_0} \notin D_i$, the line $\theta = u - \frac{\pi}{2}$ properly intersects the region $\mathcal{Z}_{D_i}$ but neither its upper nor its lower edges $\rho^+_{D_i}$ and $\rho^-_{D_i}$ (see Figure 19).*

Proof: We use the notations of the two last proofs.

Since D_i intersects $C_{s_{i_0}}$, the angle $\angle(\overrightarrow{I_1 s_{i_0}}, \overrightarrow{I_1 s_1})$ is smaller than $\pi/2$ (see Figure 20). Thus, $\|s_{i_0} s_1\| < \sqrt{2}\, R$ and the same holds for $\|s_{i_0} s_2\|$. Therefore, for any point s on the line segment $[s_1 s_2]$, $\|s_{i_0} s\| < \sqrt{2}\, R$.

As we know, $\mathcal{Z}_{D_i}$ is defined for $u \in [u_1, u_2]$. Consider any $u^* \in [u_1, u_2]$ and the corresponding point I on $C_{s_{i_0}}$. There exists s on the line segment $[s_1 s_2]$ such that the circle of radius R centered at s pass through I. Thus, one of the two vertical edges of $\mathcal{Z}_s$ lies on the line $u = u^*$. Furthermore, since $\|s_{i_0} s\| < \sqrt{2}\, R$, that vertical edge of $\mathcal{Z}_s$ is intersected by the line $\theta = u - \frac{\pi}{2}$ (see Proposition 16). This edge is contained in $\mathcal{Z}_{D_i}$ (because $\mathcal{Z}_s \subset \mathcal{Z}_{D_i}$), therefore, we have shown that $\forall u \in [u_1, u_2]$, the point $(u, u - \frac{\pi}{2})$ belongs to $\mathcal{Z}_{D_i}$. The result follows because $\mathcal{Z}_{D_i}$ is bounded by the lines $u = u_1$ and $u = u_2$. □

Proposition 29 *If $s_{i_0} \in D_i$, $\mathcal{Z}_{D_i}$ is the region shown in Figure 21. The line $\theta = u - \frac{\pi}{2}$ belongs to the relative interior of $\mathcal{Z}_{D_i}$. The curves $\rho^+_{D_i}$ and $\rho^-_{D_i}$ belong to the lines $\theta = u$, $\theta = u + \pi$, $\theta = -u + 2\gamma_i$, $\theta = -u + 2\gamma_i + \pi$.*

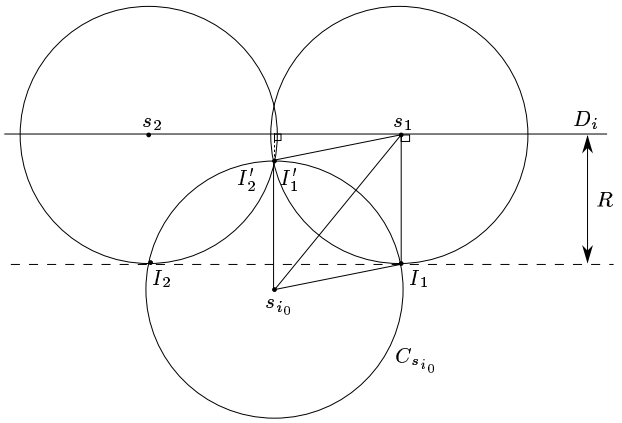

Figure 20: For the proofs of Propositions 26, 27 and 28.

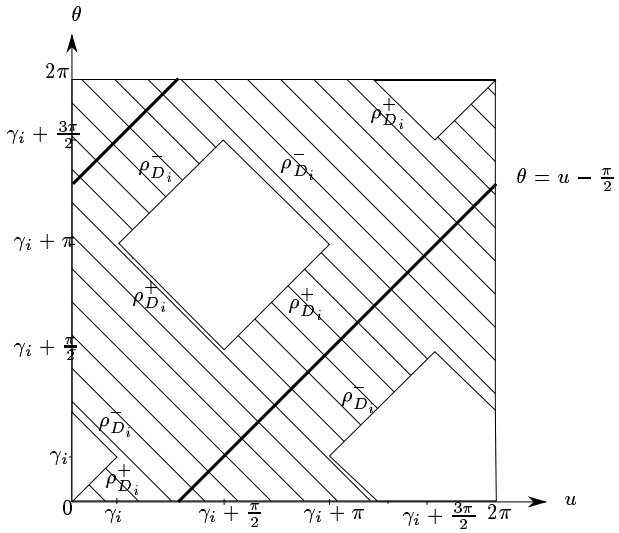

Figure 21: $\mathcal{Z}_{D_i}$ when $s_{i_0} \in D_i$.

Proof: For any $\theta \in S^1$, $\mathcal{H}_{D_i} \cap \Pi_\theta$ intersects $\mathcal{C}_{s_{i_0}}$. Moreover, according to Figure 22, for any $\theta \in [\gamma_i, \gamma_i + \frac{\pi}{2}]$ and for any $u \in [2\gamma_i - \theta, \theta + \pi]$, the point (u, θ) belongs to $(\mathcal{H}_{D_i} \cap \Pi_\theta) \cap \mathcal{C}_{s_{i_0}}$ and so belongs to $\mathcal{H}_{D_i} \cap \mathcal{C}_{s_{i_0}}$. It follows that the boundary of $\mathcal{Z}_{D_i}$ is supported by the lines $\theta = u - \pi$ and $\theta = -u + 2\gamma_i$ when $\theta \in [\gamma_i, \gamma_i + \frac{\pi}{2}]$.

$\mathcal{Z}_{D_i}$ is symmetrical with respect to the line $\theta = \gamma_i$ (see the proof of Proposition 26). Moreover, γ_i is defined modulo π, which gives the characterization of $\mathcal{Z}_{D_i}$.

For any $\theta \in S^1$, the point of $C_{s_{i_0}}$ corresponding to the parameter $\theta + \pi/2$ belongs to the half-disk $HD(s_{i_0}, \theta)$ (see Figure 22). Moreover, the point of $\mathcal{C}_{s_{i_0}}$ corresponding to the parameter $(\theta + \pi/2, \theta)$ belongs to the relative interior of $\mathcal{H}_{D_i}$. Therefore, the line $\theta = u - \frac{\pi}{2}$ belongs to the relative interior of $\mathcal{Z}_{D_i}$ (see Figure 21). □

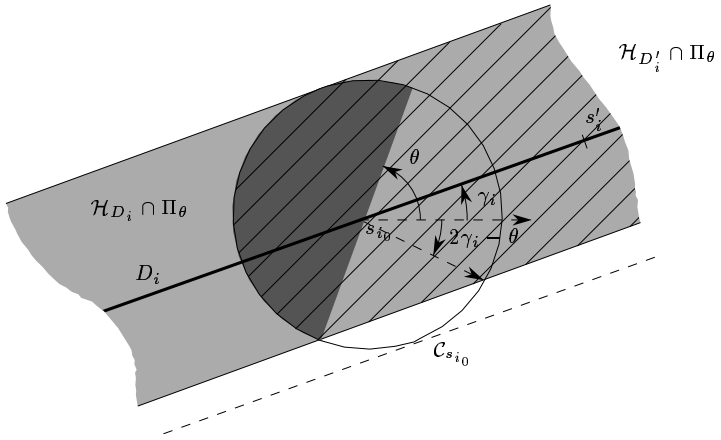

Figure 22: For the computation of $\mathcal{Z}_{D_i}$ and $\mathcal{Z}_{D_i'}$ when $s_{i_0} \in D_i$.

We now study $\mathcal{Z}_{e_i}$. Let s_i and s_i' be the two endpoints of e_i and let D_i denote the line supporting e_i. The following proposition state that the boundary of $\mathcal{Z}_{e_i}$ is made of pieces of the boundaries of $\mathcal{Z}_{s_i}$, $\mathcal{Z}_{s_i'}$ and $\mathcal{Z}_{D_i}$. we recall that $\rho^{\pm}_{D_i}$, $\rho^{\pm}_{s_i}$ and $\rho^{\pm}_{s_i'}$ denote the upper and the lower edges of $\mathcal{Z}_{D_i}$, $\mathcal{Z}_{s_i}$ and $\mathcal{Z}_{s_i'}$, respectively.

Proposition 30 *For any $i \in \{1, \ldots, n\}$, $\mathcal{C}_{s_{i_0}}$ can be split into a few vertical strips such that the region $\mathcal{Z}_{e_i}$ is bounded from above and from below by an arc of $\rho^{\pm}_{D_i}$, $\rho^{\pm}_{s_i}$ or $\rho^{\pm}_{s_i'}$. Moreover, on each strip, the line $\theta = u + \frac{\pi}{2}$ or $\theta = u - \frac{\pi}{2}$ properly intersects $\mathcal{Z}_{e_i}$ but neither its upper edge nor its lower edge.*

Proof: Let D_i' be the half straight line starting at s_i and passing through s_i'. Let $\mathcal{H}_{D_i'}$ be the helicoidal volume induced by D_i':

$$\mathcal{H}_{D_i'} = \{(P, \theta) \in I\!R^2 \times S^1 \,/\, P \in HD(s, \theta),\ s \in D_i'\}$$

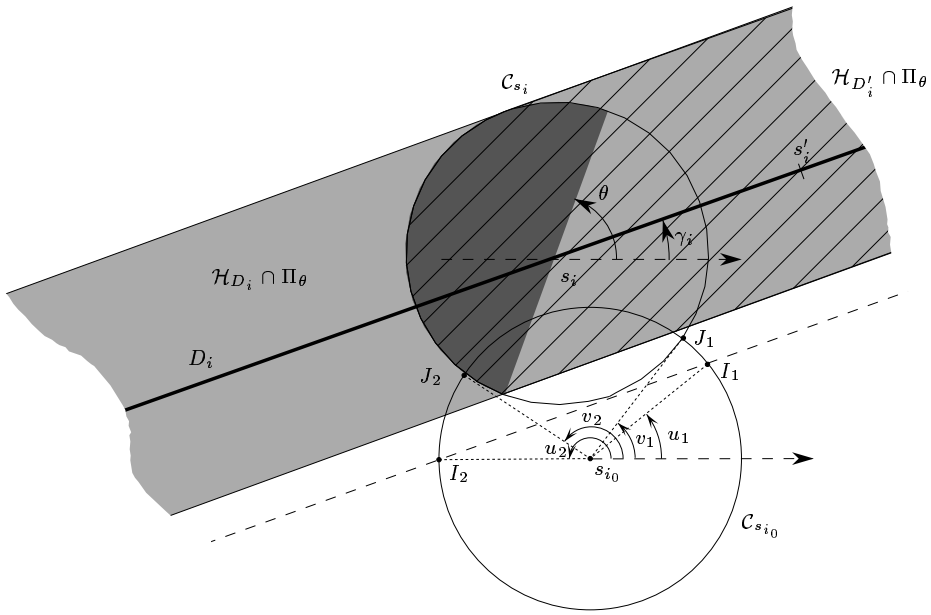

Figure 23: $\forall \theta \in [\gamma_i, \gamma_i + \pi]$, $\mathcal{H}_{D'_i} \cap \Pi_\theta$ coincides with $\mathcal{H}_{D_i} \cap \Pi_\theta$ on $\mathcal{C}_{s_i}$.

and let $\mathcal{Z}_{D'_i}$ be intersection between $\mathcal{H}_{D'_i}$ and $\mathcal{C}_{s_{i_0}}$. We show how to deduce $\mathcal{Z}_{D'_i}$ from $\mathcal{Z}_{D_i}$ and $\mathcal{Z}_{s_i}$. Then, we prove the proposition for $\mathcal{Z}_{D'_i}$ instead of $\mathcal{Z}_{e_i}$. That will yield the result because $\mathcal{Z}_{e_i}$ can be deduced from $\mathcal{Z}_{D'_i}$ and s'_i in the same way we deduce $\mathcal{Z}_{D'_i}$ from $\mathcal{Z}_{D_i}$ and $\mathcal{Z}_{s_i}$. If $\mathcal{Z}_{s_i} = \emptyset$, then $\mathcal{Z}_{D'_i} = \mathcal{Z}_{D_i}$ and Propositions 27, 28 and 29 yield the result. We suppose in the sequel that $\mathcal{Z}_{s_i} \neq \emptyset$. Furthermore, we assume that $s_i \neq s_{i_0}$; we treat this simple case at the end.

We set a few notations. Until now, γ_i denoted the angle (defined modulo π) between the x-axis and D_i. We consider here that $\gamma_i = \angle(\vec{x}, \overrightarrow{s_i s'_i})$ $[2\pi]$. Let u_1, u_2, v_1 and v_2 be the parameters of the points I_1, I_2, J_1, J_2 defined on the circle $C_{s_{i_0}}$ as follow (see Figure 23): I_1 and I_2 are the two points at distance R from D_i; J_1 and J_2 are the two points of intersection between $C_{s_{i_0}}$ and C_{s_i}; I_1, J_1, J_2 and I_2 are consecutive on $C_{s_{i_0}}$. The region $\mathcal{Z}_{s_i}$ is defined for $u \in [v_1, v_2]$. If $s_{i_0} \notin D_i$, $\mathcal{Z}_{D_i}$ is defined for $u \in [u_1, u_2]$ and otherwise, $\mathcal{Z}_{D_i}$ is defined for $u \in S^1$. Notice that $[v_1, v_2]$ is included in $[u_1, u_2]$.

We show now that $\mathcal{Z}_{D'_i}$ coincides with $\mathcal{Z}_{D_i}$ or $\mathcal{Z}_{s_i}$ on some regions of $S^1 \times S^1$:

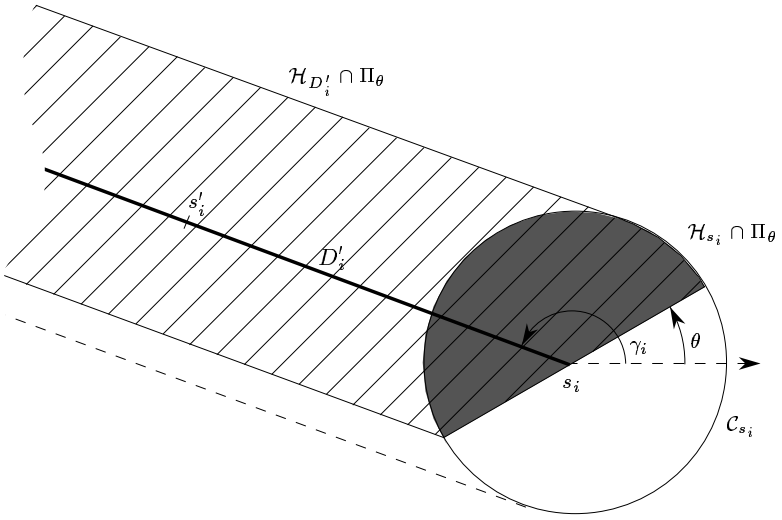

Figure 24: $\forall \theta \in [\gamma_i - \pi, \gamma_i]$, $\mathcal{H}_{D_i'} \cap \Pi_\theta$ coincides with $\mathcal{H}_{s_i} \cap \Pi_\theta$ on $\mathcal{C}_{s_i}$.

- For $\theta \in [\gamma_i, \gamma_i + \pi]$, $\mathcal{H}_{D_i'} \cap \Pi_\theta$ coincides with $\mathcal{H}_{D_i} \cap \Pi_\theta$ on $\mathcal{C}_{s_i}$ (see Figure 23). Therefore, $\mathcal{Z}_{D_i'}$ coincides with $\mathcal{Z}_{D_i}$ for $(u, \theta) \in [v_1, v_2] \times [\gamma_i, \gamma_i + \pi]$ (see Figure 25).
- For $\theta \in [\gamma_i - \pi, \gamma_i]$, $\mathcal{H}_{D_i'} \cap \Pi_\theta$ coincides with $\mathcal{H}_{s_i} \cap \Pi_\theta$ on $\mathcal{C}_{s_i}$ (see Figure 24). Therefore, $\mathcal{Z}_{D_i'}$ coincides with $\mathcal{Z}_{s_i}$ for $(u, \theta) \in [v_1, v_2] \times [\gamma_i - \pi, \gamma_i]$ (see Figure 25).
- If $s_{i_0} \notin D_i$, then, in $[u_k, v_k] \times S^1$ ($k \in \{1, 2\}$), $\mathcal{Z}_{D_i'}$ coincides either with $\mathcal{Z}_{D_i}$ or with the empty set, depending of the relatives positions of D_i' and s_i. Precisely, $\mathcal{Z}_{D_i'}$ coincides with $\mathcal{Z}_{D_i}$ in $[u_k, v_k] \times S^1$ if and only if I_k is at distance R from D_i' (see Figure 23).
- Similarly, if $s_{i_0} \in D_i$, then, in $S^1 \setminus [v_1, v_2] \times S^1$, $\mathcal{Z}_{D_i'}$ coincides with $\mathcal{Z}_{D_i}$ if $s_{i_0} \in D_i'$ and coincides with the empty set otherwise.

It follows that the computation of $\mathcal{Z}_{s_i}$ and $\mathcal{Z}_{D_i}$ provides in constant time $\mathcal{Z}_{D_i'}$. Furthermore, Propositions 27, 28 and 29 yield the result for the vertical strips $[u_1, v_1] \times S^1$ and $[v_2, u_2] \times S^1$ if $s_{i_0} \notin D_i$ (see Figure 25), and for $S^1 \setminus [v_1, v_2] \times S^1$ otherwise.

It remains to show the result for $[v_1, v_2] \times S^1$. We claim that the boundary of $\mathcal{Z}_{D_i'}$ is composed of pieces of the boundaries of $\mathcal{Z}_{D_i}$ and $\mathcal{Z}_{s_i}$. Indeed, the considerations

above yield that, for $(u,\theta) \in [v_1,v_2] \times \{\gamma_i, \gamma_i+\pi\}$, $\mathcal{Z}_{D'_i}$ coincides with $\mathcal{Z}_{D_i}$ and also with $\mathcal{Z}_{s_i}$. Thus, for $(u,\theta) \in [v_1,v_2]\times\{\gamma_i,\gamma_i+\pi\}$, $\mathcal{Z}_{D_i}$ and $\mathcal{Z}_{s_i}$ coincide (see Figure 25). Therefore, the lines $\theta=\gamma_i$ and $\theta=\gamma_i+\pi$ do not support any piece of the boundary of $\mathcal{Z}_{D'_i}$. The claim follows. If the distance between s_{i_0} and s_i is smaller than $\sqrt{2}\,R$, then we subdivide $[v_1,v_2]\times S^1$ into two or three vertical strips according to the subdivision of $\rho^{\pm}_{s_i}$ we have considered in Proposition 15. Let $U_k \times S^1$ be one of these strips. We recall that $\mathcal{Z}^k_{s_i}$ denotes the part of $\mathcal{Z}_{s_i}$included in $U_k \times S^1$ and that $\rho^{k+}_{s_i}$ and $\rho^{k-}_{s_i}$ denote its upper and lower edges ($k=1,$ 2 or 3). For convenience, if $\|s_{i_0}s_i\| \geq \sqrt{2}\,R$, we set $U_k=[v_1,v_2]$, $\mathcal{Z}^k_{s_i}=\mathcal{Z}_{s_i}$ and $\rho^{k\pm}_{s_i}=\rho^{\pm}_{s_i}$. We know by Propositions 14 or 16 that the portion of the line $\theta=u+\frac{\pi}{2}$ (or $\theta=u-\frac{\pi}{2}$) included in $U_k\times S^1$ belongs to $\mathcal{Z}^k_{s_i}$. Thus, this portion of line belongs to $\mathcal{Z}_{D'_i}$ because $\mathcal{Z}^k_{s_i} \subset \mathcal{Z}_{s_i} \subset \mathcal{Z}_{D'_i}$. That means that, in the strip $U_k\times S^1$, the line $\theta=u+\frac{\pi}{2}$ (or $\theta=u-\frac{\pi}{2}$) properly intersects $\mathcal{Z}_{D'_i}$ but neither its upper edge nor its lower edge (see Figure 25).

We consider now the case where $s_i=s_{i_0}$. Then, according to Figure 22, $\mathcal{Z}_{D'_i}$ clearly coincides with $\mathcal{Z}_{D_i}$ for $(u,\theta)\in[\gamma_i-\frac{\pi}{2},\gamma_i+\frac{\pi}{2}]\times S^1$ and coincides with $\mathcal{Z}_{s_{i_0}}$ for $(u,\theta)\in[\gamma_i+\frac{\pi}{2},\gamma_i+\frac{3\pi}{2}]\times S^1$. Thus, Propositions 10 and 29 yield the result.

Similarly, $\mathcal{Z}_{e_i}$ can be deduced from $\mathcal{Z}_{D'_i}$ and $\mathcal{Z}_{s'_i}$, which yields the result. □

Lemma 31 *Let (u_I,θ_I) be a point of $\rho^-_{D_i}$ (resp. $\rho^+_{D_i}$) and I be the point of the circle $C_{s_{i_0}}$ with parameter u_I. The point A_I (resp. B_I) at distance R from I in the direction θ_I (resp. $\theta_I+\pi$) belongs to D_i (see Figure 26).*

Proof: If D_i is the line of slope θ_I passing through I the result is obvious. We assume now that D_i is not the line of slope θ_I passing through I.

If $(u_I,\theta_I)\in\rho^-_{D_i}$, then $\exists s\in D_i$ such that $(u_I,\theta_I)\in\rho^-_s$. That means that I belongs to the radius $r_s(\theta_I+\pi)$ of $HD(s,\theta_I)$ because $\rho^-_s=\mathcal{R}^-_s\cap\mathcal{C}_{s_{i_0}}$ (see the proof of Proposition 11). Hence, s belongs to the straight line segment $[IA_I]$. If $s\neq A_I$ the half-disk robot $HD(I,\theta_I+\pi)$ properly intersects the straight line D_i and so (u_I,θ_I) belongs to the interior of $\mathcal{Z}_{D_i}$. Hence, $s=A_I$ and so, A_I belongs to D_i.

If (u_I,θ_I) is a point of $\rho^+_{D_i}$, the same arguments show that B_I belongs to D_i. □

Proposition 32 *Two curves $\rho^+_{D_i}$ and $\rho^+_{D_j}$ (or, $\rho^-_{D_i}$ and $\rho^-_{D_j}$) intersect at most twice.*

Proof: According to Lemma 31, a point on $\rho^+_{D_i}$ (resp. $\rho^-_{D_i}$) corresponds to a point on D_i. Furthermore, at most two points on $\rho^+_{D_i}$ (resp. $\rho^-_{D_i}$) correspond to the same point $A_I\in D_i$ (the two points of intersection between $C_{s_{i_0}}$ and the circle of radius

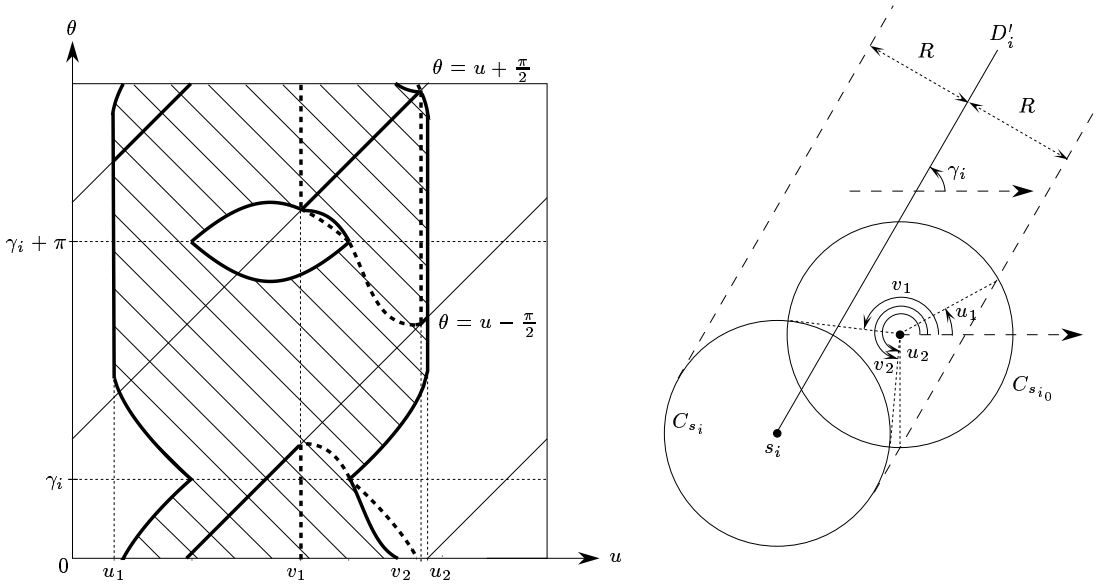

Figure 25: $\mathcal{Z}_{D'_i}$ and the relative positions of $C_{s_{i_0}}$, D_i and s_i that correspond ($\|s_{i_0}s_i\| = \sqrt{2}\,R$).

R centered at A_I). Thus, three points on $\rho^+_{D_i}$ (resp. $\rho^-_{D_i}$) define D_i. Therefore, if there exists three points of intersection between $\rho^+_{D_i}$ and $\rho^+_{D_j}$ (resp. $\rho^-_{D_i}$ and $\rho^-_{D_j}$), then $D_i = D_j$. □

Proposition 33 *Two curves $\rho^+_{D_i}$ and $\rho^-_{D_j}$ intersect at most four times.*

Proof: Let (u_I, θ_I) be a point of intersection between $\rho^+_{D_i}$ and $\rho^-_{D_j}$, and I be the point of the circle $C_{s_{i_0}}$ with parameter u_I. Lemma 31 yields that I is the midpoint of a straight line segment of length $2R$ having one end point on D_i and the other on D_j. The curve drawn by the midpoint of a ladder keeping one endpoint on D_i and the other on D_j is an ellipse. On the other hand, I belongs to the circle $C_{s_{i_0}}$. An ellipse and a circle intersect at most four times, thus there is at most four different locations for I. Moreover, (u_I, θ_I) is entirely defined by I because u_I is the parameter of I on $C_{s_{i_0}}$ and I define the position (and orientation) of the ladder and so specify θ_I (see Lemma 31). Thus, the curves $\rho^+_{D_i}$ and $\rho^-_{D_j}$ intersect at most four times. □

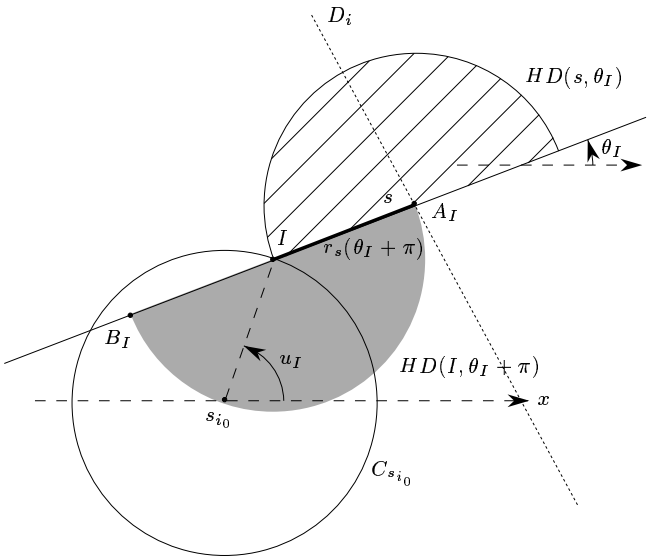

Figure 26: A_I belongs to D_i.

Proposition 34 *Two curves $\rho^{\pm}_{D_i}$ and $\rho^{\pm}_{s_j}$ intersect at most six times.*

Proof: Let (u_I, θ_I) be a point of intersection between $\rho^{-}_{D_i}$ and $\rho^{\pm}_{s_j}$, and I be the point of the circle $C_{s_{i_0}}$ with parameter u_I. Consider the curve that is the set of points at distance R from I on the line (Is_j), when I describe the circle $C_{s_{i_0}}$. This curve is a circular conchoid (see Appendix C).

According to the proof of Proposition 12, s_j belongs to the line of slope θ_I passing through I. Thus, the point A_I at distance R from I in the direction θ_I belongs to the circular conchoid defined above. Besides, A_I belongs to D_i (see Lemma 31). Thus, A_I is a point of intersection between D_i and the circular conchoid defined above. There is at most six points of intersection between a straight line and a circular conchoid (see Appendix C), and A_I define entirely (u_I, θ_I). Therefore, the curves $\rho^{-}_{D_i}$ and $\rho^{\pm}_{s_j}$ intersect at most six times. Similarly, two curves $\rho^{+}_{D_i}$ and $\rho^{\pm}_{s_j}$ intersect at most six times. □

A.2 Properties of the regions $int(\mathcal{H}_{e_i}) \cap \mathcal{C}_{s_{i_0}}$

If s_{i_0} does not belong to the line segment e_i, $int(\mathcal{H}_{e_i}) \cap \mathcal{C}_{s_{i_0}}$ is clearly equal to $int(\mathcal{Z}_{e_i})$.

If s_{i_0} belongs to e_i but is not one of its endpoints, then, according to Figure 22, $int(\mathcal{H}_{e_i}) \cap \mathcal{C}_{s_{i_0}}$ coincides with $int(\mathcal{Z}_{e_i})$ for $(u,\theta) \in S^1 \setminus \{-\frac{\pi}{2}, \frac{\pi}{2}\} \times S^1$ and coincides with the empty set for $(u,\theta) \in \{-\frac{\pi}{2}, \frac{\pi}{2}\} \times S^1$.

We now consider the case where s_{i_0} is an endpoint of e_i. Let s'_{i_0} be the other endpoint of e_i and $\gamma_{i_0} = \angle(\vec{x}, \overrightarrow{s_{i_0}s'_{i_0}})$. According to Figure 24, $int(\mathcal{H}_{e_i}) \cap \mathcal{C}_{s_{i_0}}$ clearly coincides with $int(\mathcal{H}_{e_i} \cap \mathcal{C}_{s_{i_0}}) = int(\mathcal{Z}_{e_i})$ for $(u,\theta) \in (\gamma_{i_0} - \frac{\pi}{2}, \gamma_{i_0} + \frac{\pi}{2}) \times S^1$ and $int(\mathcal{H}_{e_i}) \cap \mathcal{C}_{s_{i_0}}$ coincides with the empty set for $(u,\theta) \in [\gamma_{i_0} + \frac{\pi}{2}, \gamma_{i_0} + \frac{3\pi}{2}] \times S^1$.

Therefore, $\cup_i int(\mathcal{H}_{e_i}) \cap \mathcal{C}_{s_{i_0}}$ is equal to $\cup_{i \neq i_0} int(\mathcal{Z}_{e_i}) \cup int(\mathcal{Z}_{e_{i_0}} \cap ([\gamma_{i_0} - \frac{\pi}{2}, \gamma_{i_0} + \frac{\pi}{2}] \times S^1))$. Hence, the computation of $\cup_i int(\mathcal{H}_{e_i}) \cap \mathcal{C}_{s_{i_0}}$ comes from the computation of $\cup_{i \neq i_0} \mathcal{Z}_{e_i}$ and of $\mathcal{Z}_{e_{i_0}}$.

A.3 Construction of $\delta(\mathcal{F}_e) \cap C_{s_{i_0}}$

Let $\lambda_k(n)$ denote the maximum length of the Davenport-Schinzel sequence of order k on n symbols and $\alpha_k(n) = \lambda_k(n)/n$.

Sections A.1 and A.2 allow us to compute the contribution of the circle $C_{s_{i_0}}$ to $\delta(\mathcal{F}_e)$ in the same way we proceeded in Section 4.3.

The k_{i_0} helicoidal volumes $\mathcal{H}_{e_i}$ that intersect $\mathcal{C}_{e_{i_0}}$ can be found in $O(k_{i_0})$ time once the arrangement $\mathcal{A}_e$ of the C_{e_i} have been computed in $O(|\mathcal{A}_e| \log n)$. Thanks to Propositions 30, 32, 33 and 34, during the computation of the union of the regions $\mathcal{Z}_{e_i}$, any two curves involved in the upper and lower envelopes of the curves ρ_i^+ and ρ_i^-, intersect at most six time. Thus, the computation can be done in $O(\lambda_7(k_{i_0}) \log k_{i_0})$ time and $O(\lambda_8(k_{i_0}))$ space [Her89]. Thanks to Section A.2, the computation of $\cup_i int(\mathcal{H}_{e_i}) \cap \mathcal{C}_{s_{i_0}}$ can be done within the same time and space bounds.

Since $\mathcal{A}_e$ is the arrangement of the C_{e_i} for $i \in \{1, \ldots, n\}$, and $\mathcal{A}$ is the set of circles of radius R centered at the endpoints of each straight line segment e_i, the generalization of Section 4.3 yields the following theorem:

Theorem 35 *We can compute $\delta(\mathcal{F}_e) \cap \mathcal{A}$ and the labels of the edges of $\delta(\mathcal{F}_e)$ incident to the arcs of $\delta(\mathcal{F}_e) \cap \mathcal{A}$ in $O(|\mathcal{A}_e| \alpha_7(n) \log n)$ time and $O(|\mathcal{A}_e| \alpha_8(n))$ space.*

A.4 Contribution of the straight line segments of C_{e_i} to $\delta(\mathcal{F}_e)$

We now compute the contribution of the straight line segments of $C_{e_{i_0}}$ to $\delta(\mathcal{F}_e)$, for some $i_0 \in \{1, \ldots, n\}$. We recall some notations: l_{i_0} denotes one of the two straight line segments of $C_{e_{i_0}}$, L_{i_0} its supporting line, $\mathcal{L}_{i_0} = L_{i_0} \times S^1$ and $\mathcal{Y}_{e_i} = \mathcal{H}_{e_i} \cap \mathcal{L}_{i_0}$; D_i denotes the line supporting e_i, $\mathcal{Y}_{D_i} = \mathcal{H}_{D_i} \cap \mathcal{L}_{i_0}$ and γ_i is the angle between the (oriented) x-axis and D_i. Notice that γ_{i_0} is also the angle between the x-axis and

L_{i_0}. $\mathcal{L}_{i_0}$ is a cylinder but for convenience we will use the vocabulary of the plane when describing objects on it.

As usual, we compute $\delta(\mathcal{F}_e) \cap L_{i_0}$ by computing $\cup_i(\mathcal{H}_{e_i} \cap \mathcal{L}_{i_0})$ and $\cup_i(int(\mathcal{H}_{e_i}) \cap \mathcal{L}_{i_0})$. As in Section 4.1, we can express $\cup_i(int(\mathcal{H}_{e_i}) \cap \mathcal{L}_{i_0})$ in term of $\mathcal{Y}_{e_i}$: clearly, $int(\mathcal{H}_{e_{i_0}}) \cap \mathcal{L}_{i_0} = \emptyset$; if D_i and L_{i_0} are two parallel lines at distance R, then $int(\mathcal{H}_{e_i}) \cap \mathcal{L}_{i_0} = \emptyset$; otherwise, $int(\mathcal{H}_{e_i}) \cap \mathcal{L}_{i_0} = int(\mathcal{Y}_{e_i})$, for $i \neq i_0$. For the sake of simplicity, we assume in the following that L_{i_0} and D_i for $i \neq i_0$ are not two parallel lines. Then, $\cup_i(int(\mathcal{H}_{e_i}) \cap \mathcal{L}_{i_0}) = int(\cup_{i \neq i_0} \mathcal{Y}_{e_i})$. It follows that the contribution of L_{i_0} to $\delta(\mathcal{F}_e)$ comes from the computation of $\cup_i \mathcal{Y}_{e_i}$ and $\cup_{i \neq i_0} \mathcal{Y}_{e_i}$.

We study first $\mathcal{Y}_s = \mathcal{H}_s \cap \mathcal{L}_{i_0}$ for $s \in \mathbb{R}^2$, after which we examine $\mathcal{Y}_{D_i} = \mathcal{H}_{D_i} \cap \mathcal{L}_{i_0}$. Then, we deduce $\mathcal{Y}_{e_i}$ from $\mathcal{Y}_{D_i}$, $\mathcal{Y}_{s_i}$ and $\mathcal{Y}_{s_i'}$ where s_i and s_i' are the endpoints of e_i. We assume, for the sake of clarity, that the regions $\mathcal{Y}_s$, $\mathcal{Y}_{D_i}$ and $\mathcal{Y}_{e_i}$ under consideration are not reduced to the empty set. Notice in the sequel the typographical difference between $\varrho_s^{\pm}$ (resp. $\varrho_{D_i}^{\pm}$) that are edges of $\mathcal{Y}_s$ (resp. $\mathcal{Y}_{D_i}$) and $\rho_s^{\pm}$ (resp. $\rho_{D_i}^{\pm}$) that are edges of $\mathcal{Z}_s$ (resp. $\mathcal{Z}_{D_i}$).

Proposition 36 *The region $\mathcal{Y}_s$ is a connected region bounded by two vertical line segments of length π, and two curved edges ϱ_s^+ and ϱ_s^- which are translated copies of one another. Specifically $\varrho_s^+ = \varrho_s^- + (0, 0, \pi)$.*

Proof: The proof of Proposition 11 can easily be extended here (see Figure 27). Notice that when $s \in L_{i_0}$, the extension of the proof of Proposition 11 still holds but the curves ϱ_s^+ and ϱ_s^- are not continuous (see Figure 28). □

Proposition 37 *For any $s \notin L_{i_0}$, the line $\theta = \gamma_{i_0}$ or $\theta = \gamma_{i_0} + \pi$ properly intersects $\mathcal{Y}_s$. Furthermore, the lines $\theta = \gamma_{i_0}$ and $\theta = \gamma_{i_0} + \pi$ intersect neither ϱ_s^+ nor ϱ_s^-.*

Proof: Since $s \notin L_{i_0}$, the half-disk $HD(s, \gamma_{i_0})$ or $HD(s, \gamma_{i_0} + \pi)$ properly intersects the line L_{i_0} (if the distance between s and L_{i_0} is exactly R, then neither $HD(s, \gamma_{i_0})$ nor $HD(s, \gamma_{i_0} + \pi)$ properly intersects L_{i_0} but this case is irrelevant because then $\mathcal{Y}_s$ is reduced to a vertical segment of length π). The first claim of the proposition follows.

The edges $\varrho_s^{\pm}$ are the intersection between $\mathcal{L}_{i_0}$ and the portions $\mathcal{R}_s^{\pm}$ of the boundary of $\mathcal{H}_s$. Thus, the line $\theta = \gamma_{i_0}$ or $\theta = \gamma_{i_0} + \pi$ intersects ϱ_s^+ or ϱ_s^- if and only if the diameter of half-disk $HD(s, \gamma_{i_0})$ or $HD(s, \gamma_{i_0} + \pi)$ intersects the line L_{i_0}. As the slope of L_{i_0} is γ_{i_0} and $s \notin L_{i_0}$, the lines $\theta = \gamma_{i_0}$ and $\theta = \gamma_{i_0} + \pi$ intersect neither ϱ_s^+ nor ϱ_s^-. □

Now, we study the regions $\mathcal{Y}_{D_i}$. First, we state the following proposition which is obvious:

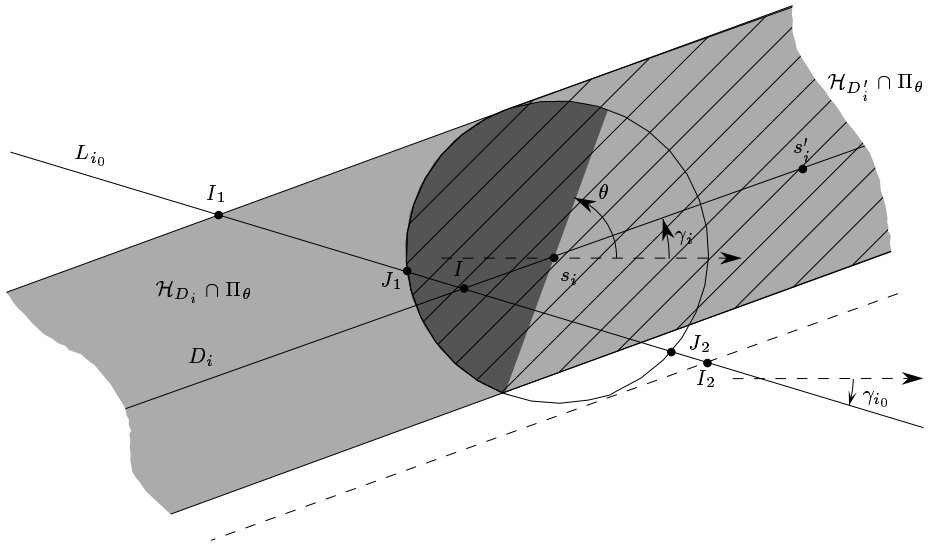

Figure 27: Section of $\mathcal{H}_{s_i}$, $\mathcal{H}_{D'_i}$ and $\mathcal{H}_{D_i}$ by the "plane" Π_θ.

Proposition 38 *The region $\mathcal{Y}_{D_{i_0}}$ is equal either to $L_{i_0} \times [\gamma_{i_0} - \frac{\pi}{2}, \gamma_{i_0} + \frac{\pi}{2}]$ or to $L_{i_0} \times [\gamma_{i_0} + \frac{\pi}{2}, \gamma_{i_0} + \frac{3\pi}{2}]$.*

Proposition 39 *For $i \neq i_0$, $\mathcal{Y}_{D_i}$ is a connected region bounded by two vertical line segments of length π, and two curved edges $\varrho^+_{D_i}$ and $\varrho^-_{D_i}$ which are symmetrical with respect to the lines $\theta = \gamma_i$ and $\theta = \gamma_i + \pi$.*

Proof: The proof of Proposition 26 can easily be extended here (see Figure 27). □

Proposition 40 *The two curves $\varrho^\pm_{D_i}$ can be subdivided into four sub-curves denoted $\varrho^{k\pm}_{D_i}$ ($k \in \{1, 2\}$) such that $\varrho^{k+}_{D_i}$ and $\varrho^{k-}_{D_i}$ are symmetrical with respect to the lines $\theta = \gamma_i$ and $\theta = \gamma_i + \pi$, and such that the line $\theta = \gamma_{i_0}$ (resp. $\theta = \gamma_{i_0} + \pi$) properly intersects the region bounded from above by $\varrho^{1+}_{D_i}$ (resp. $\varrho^{2+}_{D_i}$) and from below by $\varrho^{1-}_{D_i}$ (resp. $\varrho^{2-}_{D_i}$) but does not properly intersect these two curves.*

Proof: If $i = i_0$, the line $\theta = \gamma_{i_0}$ or $\theta = \gamma_{i_0} + \pi$ is strictly included in $\mathcal{Y}_{D_i}$ (see Proposition 38), which yields the result.

If $i \neq i_0$, then D_i and L_{i_0} intersect by hypothesis. Let I be the point where they intersect and let I_1 and I_2 be the two points of L_{i_0} at distance R from D_i (see Figure 27). The points I_1 and I_2 play symmetrical roles and similarly, γ_{i_0} is only defined modulo π in S^1. According to the choice of I_1, I_2 and γ_{i_0} in Figure 27, it comes that, in $\mathbb{R}^2 \times S^1$, $[II_1] \times \{\gamma_{i_0}\} \in \mathcal{H}_{D_i}$ and $[II_2] \times \{\gamma_{i_0} + \pi\} \in \mathcal{H}_{D_i}$. Thus, $[II_1] \times \{\gamma_{i_0}\} \in \mathcal{Y}_{D_i}$ and $[II_2] \times \{\gamma_{i_0} + \pi\} \in \mathcal{Y}_{D_i}$ because the line segments $[II_1]$ and $[II_2]$ belong to L_{i_0}. On the other hand, as $\mathcal{Y}_{D_i}$ is included in $[I_1 I_2] \times S^1$, we can subdivide the curves $\varrho^{\pm}_{D_i}$ into $\varrho^{1\pm}_{D_i}$ defined in $[II_1] \times S^1$ and $\varrho^{2\pm}_{D_i}$ defined in $[II_2] \times S^1$. According to Proposition 40, the result follows. □

Let s_i and s'_i be the endpoints of the straight line segment e_i supported by D_i.

Proposition 41 *For any $i \in \{1, \ldots, n\}$, $\mathcal{L}_{i_0}$ can be split into a few vertical strips such that the region $\mathcal{Y}_{e_i}$ is bounded from above and from below by an arc of $\varrho^{\pm}_{D_i}$, $\varrho^{\pm}_{s_i}$ or $\varrho^{\pm}_{s'_i}$. Moreover, on each strip, the line $\theta = \gamma_{i_0}$ or $\theta = \gamma_{i_0} + \pi$ is included in $\mathcal{Y}_{e_i}$.*

Proof: If neither s_i nor s'_i belongs to L_{i_0} then a straightforward extension of the proof of Proposition 30 can be applied here, according to Propositions 37, 38 and 40 (see Figure 27). Otherwise, if $s_i \in L_{i_0}$ for example, we need to notice that, on the strip $U_k \times S^1$ we deal with in the proof of Proposition 30 (here U_k is equal either to $[IJ_1]$ or to $[IJ_2]$), the lines $\theta = \gamma_{i_0}$ and $\theta = \gamma_{i_0} + \pi$ belongs to $\mathcal{Y}_{s_i}$; precisely these lines are equal to $\varrho^{+}_{s_i}$ and $\varrho^{-}_{s_i}$ on these strips (see Figure 28. Then, the straightforward extension of the proof of Proposition 30 holds here. □

Proposition 42 *If s_i and s_j are two points that are not both on L_{i_0}, then, the curves $\varrho^{\pm}_{s_i}$ and $\varrho^{\pm}_{s_j}$ intersect at most once. Otherwise, $\varrho^{\pm}_{s_i}$ and $\varrho^{\pm}_{s_j}$ may have at most two common connected part.*

Proof: Assume first that $s_i \notin L_{i_0}$. Then, the curves $\varrho^{\pm}_{s_i}$ are defined onto θ-intervals smaller than π. Indeed, $\varrho^{+}_{s_i}$ (resp. $\varrho^{-}_{s_i}$) is the intersection between $\mathcal{R}^{+}_{s_i}$ (resp. $\mathcal{R}^{-}_{s_i}$) and $\mathcal{L}_{i_0}$, and the radius $r_i(\theta)$ (resp. $r_i(\theta + \pi)$) intersects the line L_{i_0} on a θ-interval smaller than π because $s_i \notin L_{i_0}$. Now, the proof of Proposition 12 can easily be extended here.

If s_i and s_j are both on L_{i_0}, then, according to Figure 28 the result is obvious. □

Lemma 43 *Let $(I, \theta_I) \in L_{i_0} \times S^1$ be a point of $\varrho^{-}_{D_i}$ (resp. $\varrho^{+}_{D_i}$). The point A_I (resp. B_I) at distance R from I in the direction θ_I (resp. $\theta_I + \pi$) belongs to D_i.*

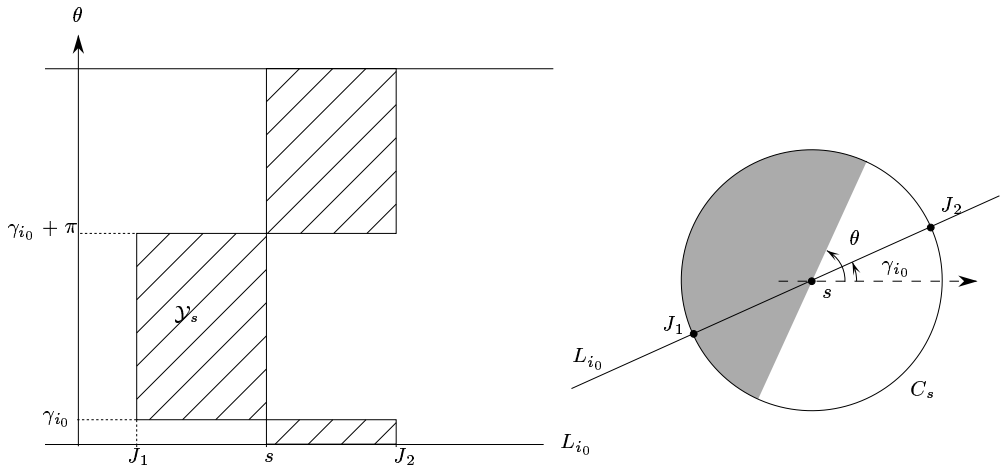

Figure 28: $\mathcal{Y}_s$ and the relative positions of C_s and L_{i_0} that correspond ($s \in L_{i_0}$).

Proof: The proof is the same as the proof of Lemma 31. □

Proposition 44 *Two curves $\varrho^{\pm}_{D_i}$ and $\varrho^{\pm}_{D_j}$ intersect at most twice.*

Proof: Two curves $\varrho^{+}_{D_i}$ and $\varrho^{+}_{D_j}$ (or, $\varrho^{-}_{D_i}$ and $\varrho^{-}_{D_j}$) intersect at most twice because the proof of Proposition 32 can be applied here. Since a straight line intersects an ellipse at most twice, the proof of Proposition 33 yields the result. □

Proposition 45 *Two curves $\varrho^{\pm}_{D_i}$ and $\varrho^{\pm}_{s_j}$ intersect at most four times.*

Proof: The proof is similar to the proof of Proposition 34. Here, the maximum number of intersection between $\varrho^{\pm}_{D_i}$ and $\varrho^{\pm}_{s_j}$ is the maximum number of intersection between a straight line and a conchoid which is four (see Appendix B). □

The computation of $\delta(\mathcal{F}_e) \cap L_{i_0}$ can be done in the same way as in Section 4.3. Here, the two sets Ω_1 and Ω_2 introduced in Section 4.3 are induced by the lines $\theta = \gamma_{i_0}$ and $\theta = \gamma_{i_0} + \pi$ instead of $\theta = u \pm \pi/2$.

According to Section A.3 and to Propositions 42, 44 and 45, the contribution of L_{i_0} to $\delta(\mathcal{F}_e)$ can be computed in $O(\lambda_5(k_{i_0})\log(k_{i_0}))$ time and $O(\lambda_6(k_{i_0}))$ space. Therefore, if $\mathcal{B}$ denotes the arrangement of straight line segments of $\mathcal{A}_e$, it comes the following theorem:

Theorem 46 *We can compute $\delta(\mathcal{F}_e) \cap \mathcal{B}$ and the labels of the edges of $\delta(\mathcal{F}_e)$ incident to the arcs of $\delta(\mathcal{F}_e) \cap \mathcal{B}$ in $O(|\mathcal{A}_e|\alpha_5(n)\log n)$ time and $O(|\mathcal{A}_e|\alpha_6(n))$ space.*

B Conchoids

A conchoid is the curve drawn by the endpoint P of a straight line segment $[PQ]$ of length L when Q moves along a fixed straight line D and when the line PQ contains a fixed point O (see Figure 29).

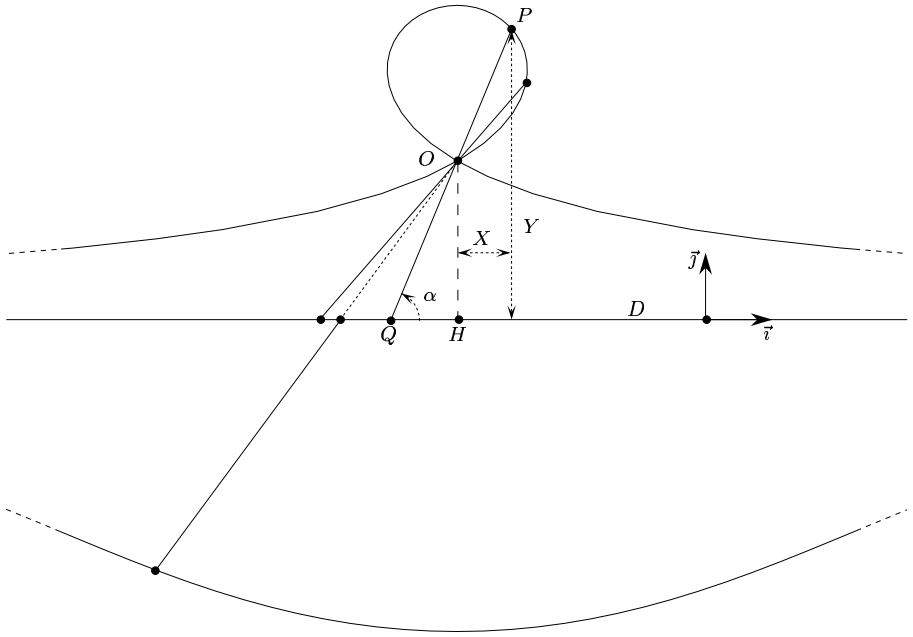

Figure 29: Conchoid.

Let H be the orthogonal projection of O onto D and $h = \|OH\|$. We give a parametric equation of the conchoid in the orthonormal reference frame $(H, \vec{\imath}, \vec{\jmath})$ (see Figure 29). Let (X, Y) denote the coordinates of P in this reference frame. Let α denote the angle $\angle(\vec{\imath}, \overrightarrow{QP})$. We have:

$$\begin{cases} X = L\cos(\alpha) - \dfrac{h}{\tan(\alpha)} \\ Y = L\sin(\alpha) \end{cases}$$

Considering $t = \tan(\alpha/2)$, we obtain:

$$\begin{cases} X = \dfrac{ht^4 - 2Lt^3 + 2Lt - h}{2t(1+t^2)} \\ Y = \dfrac{2Lt}{1+t^2} \end{cases}$$

A straight line and a conchoid intersect at most four times because any equation $aX + bY + c = 0$ yields a polynomial of degree at most four in t.

Lemma 47 *The line segment $[PQ]$ is tangent to the conchoid at P if and only if $P = O$.*

Proof: The system above yields:

$$\begin{cases} \dot{X} = -L\dot{\alpha}\sin(\alpha) + \dfrac{h\dot{\alpha}}{\sin^2(\alpha)} \\ \dot{Y} = L\dot{\alpha}\cos(\alpha) \end{cases}$$

The line segment $[PQ]$ is tangent to the conchoid at P if and only if $\frac{\dot{X}}{\dot{Y}} = \cot(\alpha)$. We have:

$$\frac{\dot{X}}{\dot{Y}} - \cot(\alpha) = -\tan(\alpha) + \frac{h}{L\sin^2(\alpha)\cos(\alpha)} - \cot(\alpha) = \frac{-1}{\sin(\alpha)\cos(\alpha)}\left(1 + \frac{h}{L\sin(\alpha)}\right).$$

As $\sin(\alpha) = \frac{h}{L}$ if and only if $P = O$ (see Figure 29), the claim is proved. □

Lemma 48 *Given two straight lines D_1 and D_2, and a line segment $[P_1P_2]$ of length L such that $P_1 \in D_1$ and $P_2 \in D_2$, there exists at most one point O on $[P_1P_2]$ such that the conchoid $\mathcal{K}_1$ induced by D_1, O and L is tangent to D_2 at P_2. We can decide if such a point O exists and, in case, compute its position, in constant time. Moreover, the conchoid $\mathcal{K}_2$ induced by D_2, O and L is tangent to D_1 at P_1 (see Figure 30).*

Proof: Consider without loss of generality, D_1 supported by the x-axis; let (X, Y) denote the coordinates, in the frame described above, of the point P_2 on the conchoid induced by D_1, O and L, and let s denote the slope of D_2. The conchoid induced by D_1, O and L that is tangent to D_2 at P_2 must verify that $\dot{Y}/\dot{X} = s$. Thus,

$$\frac{L\cos(\alpha)}{-L\sin(\alpha) + \dfrac{h}{\sin^2(\alpha)}} = s.$$

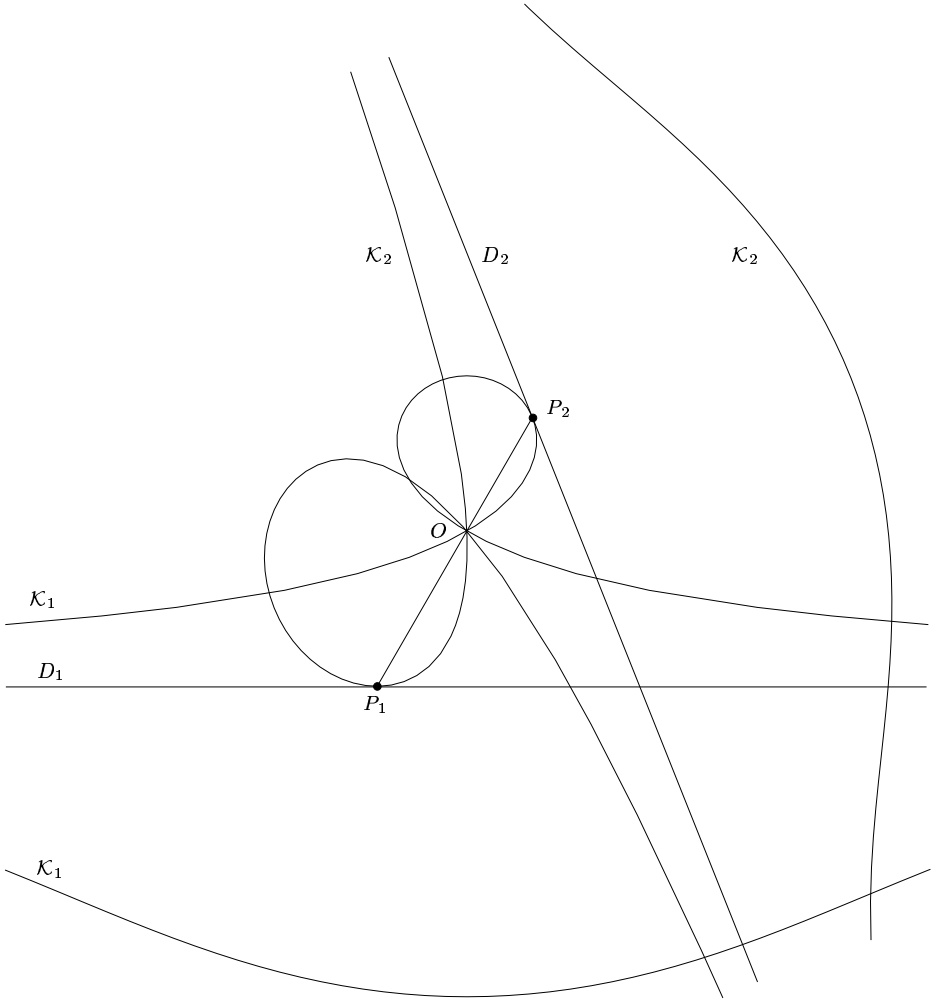

Figure 30: For the Lemma 48.

It comes h in term of L, α and s. Thus, for D_1, D_2, P_1 and P_2 fixed, O comes as the intersection (if existing) of the line segment $[P_1P_2]$ and of the horizontal straight line of equation $(Y = h)$. Therefore, there exists at most one such a point O and, we can decide if it exists and, in case, compute its position, in constant time.

We show now, that the conchoid $\mathcal{K}_2$ induced by D_2, O and L is tangent to D_1 at P_1 (see Figure 30). Indeed, assume for a contradiction that $\mathcal{K}_2$ is not tangent to D_1 at P_1. We show that, in any neighborhood of P_1, there exists a point $P_1^* \in D_1$ such that the line segment $[P_1^* P_2^*]$ of length L, that contains O, intersects D_2. That will yield the claim. Since $P_1 \in \mathcal{K}_2$, $\mathcal{K}_2$ properly intersects D_1 at P_1. Thus, there exists, in any neighborhood of P_1, a point $P_1^* \in D_1$ such that the line segment, of length L passing through O and touching D_2, contains P_1^*. Therefore, the line segment, of length L passing through O and touching D_1 at P_1^*, intersects D_2. That implies that $\mathcal{K}_1$ intersects D_2 and contradicts our assumption. □

C Circular conchoids

A circular conchoid is the curve drawn by the endpoint P of a straight line segment $[PQ]$ of length L when Q moves along a fixed circle C and when the line PQ contains a fixed point O (see Figure 31). Let O_1 and R denote the center and the radius of C.

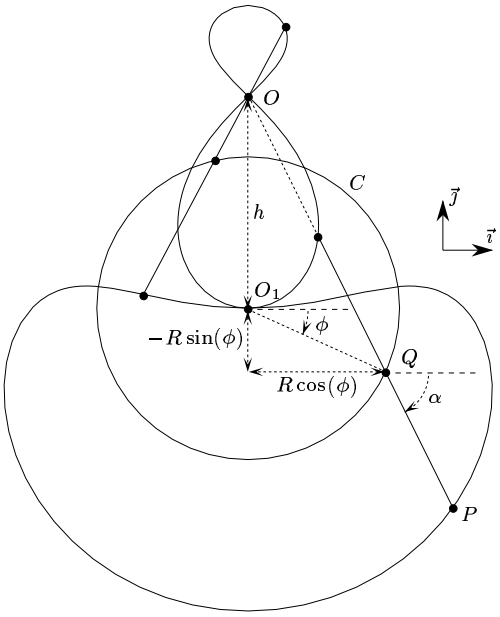

Figure 31: Circular conchoid (when $L = R$).

We give a parametric equation of the circular conchoid in the orthonormal reference frame $(O_1, \vec{\imath}, \vec{\jmath})$ (see Figure 31).

Let (X, Y) denote the coordinates of P in this reference frame. Let α denote the angle $\angle(\vec{\imath}, \overrightarrow{QP})$, ϕ the angle $\angle(\vec{\imath}, \overrightarrow{O_1Q})$ and h the Euclidean distance between O and O_1. We have:

$$\begin{cases} X = R\cos(\phi) + L\cos(\alpha) \\ Y = R\sin(\phi) + L\sin(\alpha) \end{cases}$$

where $\cos(\alpha)$ (resp. $-\cos(\alpha)$) is equal to

$$\frac{-R\cos(\phi)}{\sqrt{R^2\cos^2(\phi) + (h - R\sin(\phi))^2}} = \frac{-R\cos(\phi)}{\sqrt{R^2 + h^2 - 2hR\sin(\phi)}}$$

when O belongs (resp. does not belong) to the half straight line ending at Q and passing through P. Similarly, $\sin(\alpha)$ (resp. $-\sin(\alpha)$) is equal to

$$\frac{h - R\sin(\phi)}{\sqrt{R^2\cos^2(\phi) + (h - R\sin(\phi))^2}} = \frac{h - R\sin(\phi)}{\sqrt{R^2 + h^2 - 2hR\sin(\phi)}}$$

when O belongs (resp. does not belong) to the half straight line ending at Q and passing through P.

With $t = \tan(\phi/2)$, we obtain:

$$\begin{cases} X = \dfrac{1}{1+t^2}\left(R(1-t^2) \mp \dfrac{LR(1-t^2)}{\sqrt{f(t)}}\right) \\ Y = \dfrac{1}{1+t^2}\left(2Rt \pm \dfrac{Lh(1+t^2) - 2LRt}{\sqrt{f(t)}}\right) \end{cases}$$

where:

$$f(t) = R^2 + h^2 - \frac{4hRt}{1+t^2}.$$

A straight line and a circular conchoid intersect at most six times because any equation $aX + bY + c = 0$ yields a polynomial of degree at most six in t.

References

[BDDP95] J.-D. Boissonnat, O. Devillers, L. Donati, and F. Preparata. Motion planning of legged robots: the spider robot problem. *Internat. J. Comput. Geom. Appl.*, 5(1–2):3–20, 1995.

[DD90] M. Dickerson and R. L. Drysdale. Fixed radius search problems for points and segments. *Inform. Process. Lett.*, 35:269–273, 1990.

[Her89] J. Hershberger. Finding the upper envelope of n line segments in $O(n \log n)$ time. *Inform. Process. Lett.*, 33:169–174, 1989.

[HK91] S. Hirose and O. Kunieda. Generalized standard foot trajectory for a quadruped walking vehicle. *The International Journal of Robotics Research*, 10(1), February 1991.

[HNKU84] S. Hirose, M. Nose, H. Kikuchi, and Y. Umetani. Adaptive gait control of a quadruped walking vehicule. In *Int. Symp. on Robotics Research*, pages 253–277. MIT Press, 1984.

[JW89] J.Bares and W.L.Whittaker. Configuration of an autonomous robot for mars exploration. In *World Conference on Robotics Research*, pages 37–52, 1989.

[KS90] K. Kedem and M. Sharir. An efficient motion planning algorithm for a convex rigid polygonal object in 2-dimensional polygonal space. *Discrete Comput. Geom.*, 5:43–75, 1990.

[KST97] K. Kedem, M. Sharir, and S. Toledo. On critical orientations in the Kedem-Sharir motion planning algorithm for a convex polygon in the plane. *Discrete Comput. Geom.*, 17:227–240, 1997.

[RR84] Special issue on legged locomotion. *Internat. J. Robot. Res.*, 3(2), 1984.

[RR90] Special issue on legged locomotion. *Internat. J. Robot. Res.*, 9(2), 1990.

[Sha91] M. Sharir. On k-sets in arrangements of curves and surfaces. *Discrete Comput. Geom.*, 6:593–613, 1991.

[SS87] S. Sifrony and M. Sharir. A new efficient motion-planning algorithm for a rod in two-dimensional polygonal space. *Algorithmica*, 2:367–402, 1987.

[Tur91] V. Turau. Fixed-radius near neighbors search. *Inform. Process. Lett.*, 39:201–203, 1991.

Unité de recherche INRIA Lorraine, Technopôle de Nancy-Brabois, Campus scientifique,
615 rue du Jardin Botanique, BP 101, 54600 VILLERS LÈS NANCY
Unité de recherche INRIA Rennes, Irisa, Campus universitaire de Beaulieu, 35042 RENNES Cedex
Unité de recherche INRIA Rhône-Alpes, 655, avenue de l'Europe, 38330 MONTBONNOT ST MARTIN
Unité de recherche INRIA Rocquencourt, Domaine de Voluceau, Rocquencourt, BP 105, 78153 LE CHESNAY Cedex
Unité de recherche INRIA Sophia Antipolis, 2004 route des Lucioles, BP 93, 06902 SOPHIA ANTIPOLIS Cedex

Éditeur
INRIA, Domaine de Voluceau, Rocquencourt, BP 105, 78153 LE CHESNAY Cedex (France)
ISSN 0249-6399